ELSEVIER

Contents lists available at ScienceDirect

# Geomechanics for Energy and the Environment

journal homepage: www.elsevier.com/locate/gete



# An integral approach using InSAR and data assimilation to disentangle and quantify multi-depth driven subsidence causes in the Ravenna coastland, Northern Italy

Manon Verberne a,b,c,\*, Pietro Teatini b, Kay Koster c, Peter Fokker a,c, Claudia Zoccarato b

- <sup>a</sup> Faculty of Geosciences, Utrecht University, Utrecht, the Netherlands
- b University of Padova, Faculty of Civil, Environmental and Architectural Engineering, Padova, Italy
- <sup>c</sup> TNO Geological Survey of the Netherlands, Utrecht, the Netherlands

#### ARTICLE INFO

### Keywords: Subsidence Data assimilation Gas extraction Soil InSAR Inversion Coastal

#### ABSTRACT

Land subsidence in the Ravenna area (Italy) was a hydrogeological hazard until the end of last century. Although subsidence reduced during the last decades, the area is still experiencing vertical displacements. Understanding their drivers is challenging. Land subsidence magnitude and distribution must be interpreted with a combination of geological factors and human activities. This study integrates various datasets, subsidence observations, and subsidence models to evaluate the contributions of three main causes; building related, shallow subsurface processes and deep subsurface processes. The model result was optimized using Interferometric Synthetic Aperture Radar. The highest subsidence rates, of over 10 mm/year, were found at locations where multiple causes have an effect. The results of building-related subsidence indicate that subsidence rates associated with industrial buildings are twice as high as for residential buildings. This difference is even more pronounced in lagoonal and reclaimed areas. Shallow causes, associated with overburden weight on tidal deposits and drainage of reclaimed land, cause significant subsidence along the coast. Deep causes, by offshore gas extraction, contribute to subsidence along parts of the coast, with a decreasing trend over time. Other factors, such as lowlying farmland drainage, (historical) groundwater extraction and compaction of Quaternary deposits are not specifically addressed because of their small contribution to the total subsidence during the time period considered. This study underscores the importance of a comprehensive approach that considers the interplay between geomorphology and geology, industrialization, urbanization, and fluid extraction. Geotechnical assessments and improved subsidence models, incorporating localized data on buildings and subsurface fluid withdrawals, are crucial for developing effective mitigation strategies.

# 1. Introduction

Land subsidence can lead to a wide range of negative consequences, including damage to infrastructure such as roads, buildings, and pipelines; increased flood risk due to reduced surface elevations relative to the sea level, salinization of groundwater, and loss of agricultural productivity. <sup>23,31,65</sup> In urban areas it compromises the integrity of built environments, while in rural and deltaic zones it disrupts ecosystems and impairs drainage networks, exacerbating flood vulnerability. <sup>52</sup>

Coastal plains and deltas are particularly susceptible to subsidence due to a combination of factors.  $^{41,62,69}$  These regions face significant flood risks from relative sea-level rise and often have high population densities.  $^{51}$  The subsurface typically consists of thick, compressible soil

layers that are prone to subsidence,  $^{41,46}$  and the extraction of natural fluids from the subsurface, which is a common practice in these areas, can further exacerbate the issue.  $^{31,50,75}$ 

Subsidence is often the result of multiple spatially overlapping processes, making it challenging to determine the contribution of each process when only the total subsidence response is measured at the surface. Understanding the individual contributions is crucial for the development of effective mitigation strategies, especially in deltas and coastal plains.

Many studies highlight the importance of addressing land subsidence as the sum of all concurring processes in a certain area (e.g. <sup>32,47,17</sup>), but it is far from common practice in subsidence research. <sup>78</sup> Most studies either simply compare satellite observations to expected subsidence (e.

<sup>\*</sup> Corresponding author at: Faculty of Geosciences, Utrecht University, Utrecht, the Netherlands. *E-mail addresses*: manon.verberne@tno.nl, m.a.m.verberne@uu.nl (M. Verberne).

g. <sup>68,88</sup>), or correlate subsurface properties to subsidence rates by using machine learning techniques (e.g. <sup>42</sup> and <sup>2</sup>). Such approaches do however not quantify the physics of the various sources of subsidence. This study addresses this knowledge gap by adopting a process-based approach to land subsidence in a data assimilation framework, aiming to disentangle the multiple contributing factors underlying the total surface displacement.

Data assimilation offers a promising framework to integrate heterogeneous observations and disentangle the contributions of multiple processes within a single model domain whilst incorporating the multiple physical relations of subsidence. Zoccarato et al.,  $^{89}$  Fokker et al.,  $^{30}$  and Gazzola et al.  $^{36}$  utilized data assimilation techniques to enhance subsidence modelling of gas-extraction-related subsidence. Verberne et al.  $^{81,79}$  applied data assimilation to examine the subsidence contribution of processes in Holocene coastal deposits. These studies collectively underscore the power of this technique in refining subsidence models and developing effective mitigation strategies by leveraging high-resolution data and advanced numerical techniques.

This contribution advances previous integrated data assimilation studies on subsidence by incorporating both shallow and deep sources. This represents a significant step toward developing an effective methodology capable of capturing the full range of subsidence-driving processes across different depths. Multiple subsidence-driving processes are combined in a single optimization procedure to fit the model outcome to the surface movement estimates from InSAR data. The aim is to understand the spatiotemporal pattern of the current subsidence drivers and provide physical parameters that can directly be implemented to predict subsidence and subsequently mitigate the consequences effectively.

The proposed framework is applied to the coastal plain of Ravenna, on the coastland of the Po River plain in Italy (Fig. 1), which exemplifies a region with a complex land subsidence history resulting from various causes, including aquifer overexploitation, urbanization, industrialization, drainage, gas extraction from deep reservoirs, peatland oxidation, shallow and deep sediment compaction, and tectonics<sup>7,33,71</sup>. Land subsidence, which mainly occurred from the 1950s to the early 2000s, is threatening the structural integrity of cultural heritage sites in the region, generally affecting the livelihood of people and the natural

environment of the Po plain. 71 Although subsidence in the region has been extensively studied over the past decades, most research has primarily focused on groundwater and resource extraction (e.g. 7.66,71,72). However, groundwater withdrawal has been reduced considerably over the past decade, and other drivers of subsidence in the coastland have grown in relative importance. We therefore aim to identify the driving parameters of current subsidence. Parameter quantification and subsidence contribution analysis are more challenging with recent, smaller displacement rates compared to pre-1990s data, when significant subsidence due to aquifer over-exploitation affected the area. 71,72 We focus on the combined effect of the main causes over the past decade and offer new insights into the most recent drivers of subsidence.

This study primarily relies on freely available or commonly accessible datasets, making the approach readily transferable to other regions. By integrating multiple datasets, we have been able to model and quantify subsidence due to various drivers: (i) building load (distinguishing between residential and industrial structures), (ii) shallow processes occurring within Holocene deposits across different geomorphological classes, and (iii) deep causes related to gas extraction. In the following sections we detail the methodology, datasets included, and data processing techniques used. The results and discussion sections highlight the complexity of the subsidence problem in the region and provide a quantification of the effects of the main subsidence processes acting in the region. Understanding these complex interactions is crucial for formulating effective mitigation strategies and ensuring the stability and sustainability of the Ravenna area in the near future.

### 2. Study area

The Ravenna coastal area belongs to the southeastern part of the Po River plain, Italy (Fig. 1). It is composed of wetlands, lagoons, industrial areas, reclaimed land, agricultural land, rivers, canals, and the city of Ravenna itself. Subsidence consequently occurs in a complex pattern, with variations in space and time relating to both natural and anthropogenic environments. The area, like many other coastal areas, is vulnerable due to the combination of an increase in mean sea level and loss of surface elevation. <sup>71</sup> For this reason, the different mechanisms of

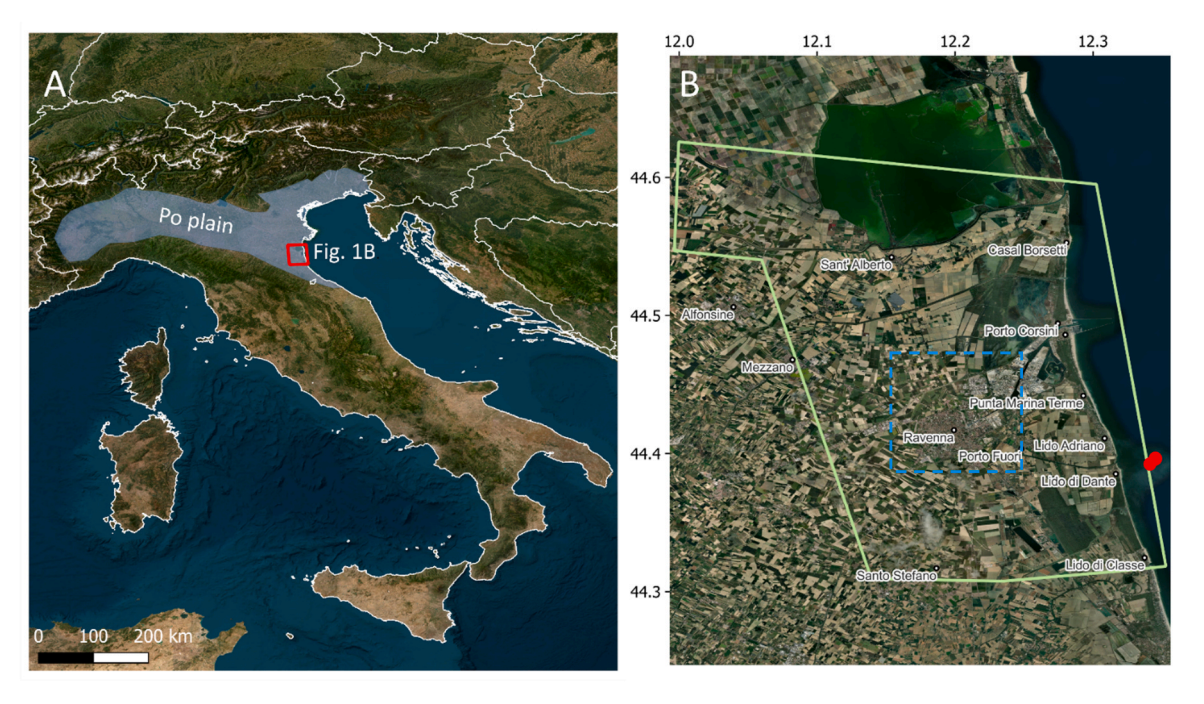


Fig. 1. A: Map of Italy, showing the outline of the Po plain and the location of the research area. B: Study area with the name of the main urban centers (coordinate system WGS-84). The small red dots in the southeast are the CH4 production platforms. The dashed blue box refers to the area around the city of Ravenna shown in Fig. 3.

subsidence acting in the area have been studied extensively over the past decades.  $^{7,35,33,63,66,72}$ 

The geological history influencing current subsidence patterns commenced with the deposition of low-permeable alluvial confining clay beds during Pleistocene sea-level low stands. These deposits are at present characterized by their stiff and overconsolidated mechanical properties. During the mid-Holocene the area drowned under the influence of global sea-level rise, <sup>60</sup> depositing tidal and fluvial sediments at the base of the coastal sequence. A beach barrier-lagoon system formed during sea-level highstand, grading into alluvial plain deposits formed by fluvial and tidal processes in the back-barrier plain. The maturation of the beach barrier was followed by a progradational movement, resulting in a second, more seaward positioned barrier, as a result of an increase in sediment supply due to large deforestation during the rise of the classical civilizations. <sup>4,14,44</sup>

This deforestation marks the first period of major anthropogenic influence on the Po delta and dates back to the 3rd century AD, when the rise of classical civilizations led to a spread in agricultural activity in Europe. This resulted in an increase in soil erosion and hence a major burst in progradation of the delta. <sup>45</sup> Since that time, the area has undergone substantial changes in land and groundwater use, resulting in anthropogenically driven land subsidence. Accounts of early subsidence are based on archaeological findings on buried beach barriers. They indicate a subsidence rate of 2–3 mm/year over the last 2500 years. <sup>35,61,71,77</sup>

Starting from the period after World War I, the anthropogenic influence on subsidence became even more prominently visible, due to channeling rivers, damming, progressive reclamation of the lagoon areas, urbanization and an increase in industry. An important consequence of this was the reduction of sediment transport to the coast. Therefore, land subsidence was not counterbalanced by sediment deposition. A few millimeters per year of subsidence increased to 110 mm/year in 1972 and 1973, largely due to groundwater extraction (e.g. <sup>19,9</sup>). From the seventies onwards, major problems started to arise, such as floodings in the city center of Ravenna and of coastal villages. This threatens the cultural heritage sites in the area. Additionally, floods threatened lagoon ecosystems by increasing salinization.

Many research activities over the past decades have focused on subsidence processes and mitigation to be able to preserve historic sites, coastal environment, and infrastructure. It was established that the main driver of subsidence in the 1960s and 1970s was groundwater extraction. <sup>19,72,9</sup> The gas extraction from on- and offshore gas fields contributed as well, but only locally and with smaller values. <sup>34</sup> Recent measurements (e.g., <sup>27,83</sup>) show that land subsidence significantly reduced to a few mm/year in the largest part of the coastal area, as the main onshore fluid extraction activities have ceased. <sup>10</sup> With the major cause of subsidence identified and addressed, the research focus shifted away from subsidence in the Ravenna area. However, some spots in the area still exhibit subsidence rates of over 10 mm/year.

### 3. Materials and methods

In this study, we combine various data sources, subsidence models, and a data assimilation approach to quantify and map the contributions of different subsidence processes to the total observed subsidence. Below we discuss all data sources, the forward models, and the integration step with data assimilation. The datasets used in this study are (i) a database for land-use and building information – Global Human Settlement Layer, (ii) a soil texture map, (iii) Cone Penetration Tests (CPTs), (iv) an estimate of land subsidence by gas extraction, (v) InSAR-derived displacement estimates over time, and (vi) a geomorphological mapping product based on literature and processed CPT data.

The methodology is summarized in Fig. 2. The datasets serve as the input to the data assimilation approach, by which we integrate three distinct subsidence causes to determine the total effect: (1) building-induced subsidence, (2) subsidence caused within the shallow (Holocene) subsurface, and (3) subsidence caused within the deep subsurface by hydrocarbon production.

# 3.1. Global Human Settlement Layer (GHSL)

The Global Human Settlement Layer (GHSL)<sup>25</sup> projects data on maps that describe the human presence on Earth. The dataset is formed by automatic data analytics and data extraction from large amounts of heterogeneous geospatial information, including satellite images, census data, crowd sourced and volunteered geographic information sources. The GHSL data package, which was released in 2023, contains data on buildings, building use, land-use, population, and degree of urbanization. From the dataset we have used the GHS-BUILT-V R2023A<sup>25</sup> dataset to derive the change in built-up volume on a regular  $100 \times x100$  m grid from 1975 onwards in five-year intervals.<sup>54</sup> From GHS-BUILT-C R2023A<sup>25</sup> dataset we have derived the settlement characteristics, to distinguish between residential buildings and offices versus buildings for industrial purposes. The most dominant building purpose determines the building category in the  $100 \times 100$  m grid-cells.<sup>53</sup>

# 3.2. Soil texture

The Geological, Seismic and Soil Survey of the Emilia-Romagna region (GSSS-ER) has constructed a map of the soil texture (0–30 cm) on a scale of 1:50.0000, represented by particle distribution. The map is based on the interpolation from field samples in the soil database of the Emilia-Romagna region. Twelve textural soil classes have been identified, given the content of clay, sand, and silt according to the USDA classification of soil texture.

We simplified the data into four classes, for clarity and generalization of the behavior in the region. Fig. 3 shows the resulting soil texture classification. This classification has been used in the determination of the different geomorphological classes of the research area (Section 3.6).

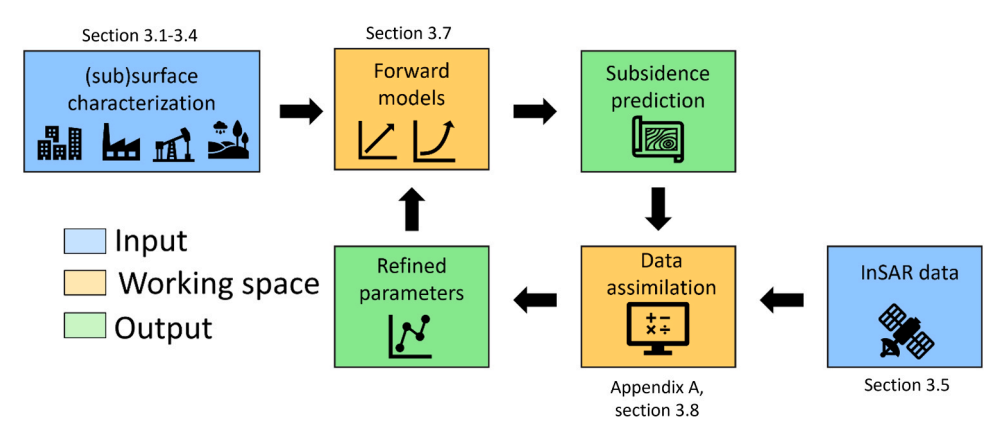


Fig. 2. Methodology depicted in a workflow diagram.

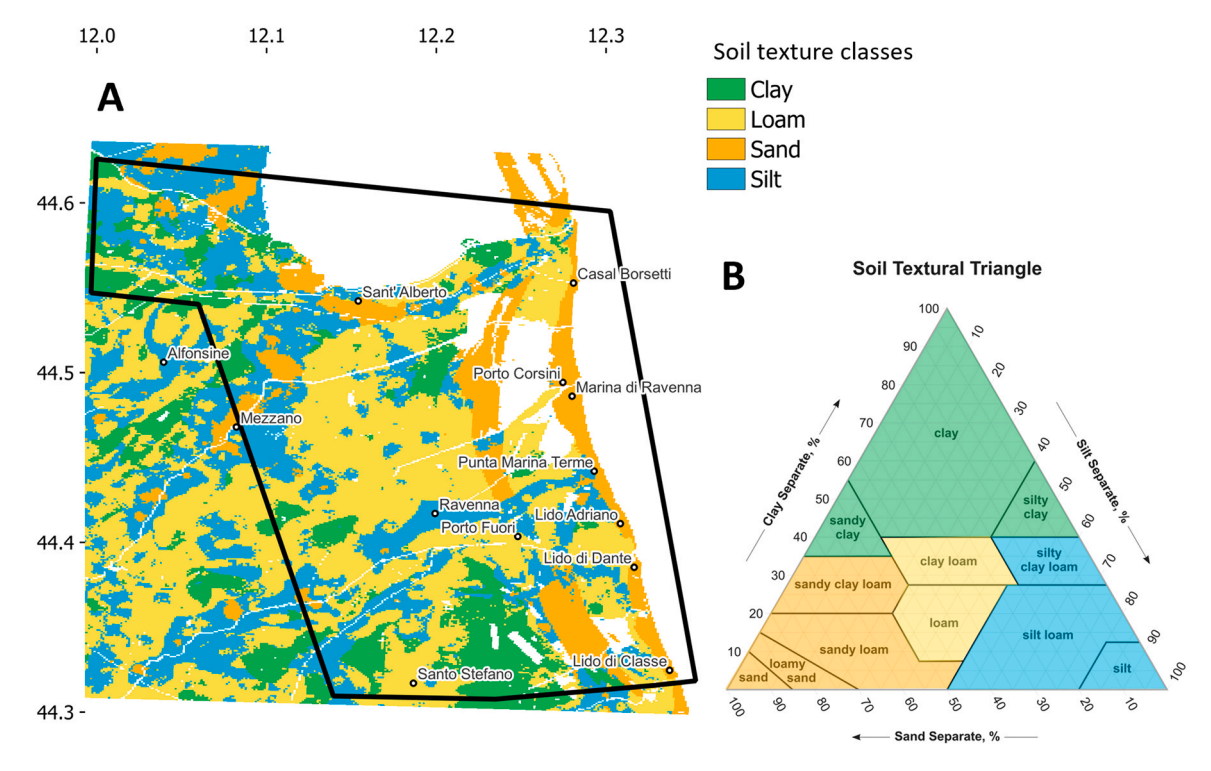


Fig. 3. A: Soil texture map for the research area. Coordinate system: WGS-84. B: Simplified soil texture classes for the research area based on USDA classification.<sup>49</sup>).

# 3.3. Cone penetration test

The Cone Penetration Test (CPT) is a geotechnical site investigation technique applied worldwide.  $^{43}$  The CPT is strongly related to the composition of the subsurface and can be translated into soil types with the use of empirical relations.  $^{58,59}$ 

The CPT data for this study (Fig. 4 a) has been derived from the open-source databank of the GSSS-ER. <sup>57</sup> We selected nine sections perpendicular to the coastline in the study area to construct a geomorphological mapping product (Fig. 4). For each section, we projected all the CPT locations within 500 m onto the sections. The CPT data were translated into soil types by using the Robertson <sup>58</sup> classification chart.

The sections show that the depth of the top of the sandy beach barrier and the total thickness of the sediments with compaction potential above it (lagoon and alluvial plain) vary substantially. Fig. 5 plots three of the nine sections to exemplify this behavior. The thicknesses of the compressible sediments dependents on the depth of the sandy beach barrier if present or on the top depth of deposits of-Pleistocene age.

The thickness of the alluvial plain, consisting of compressible soil, varies significantly (Fig. 6). To account for the effect of this on the total subsidence, the thickness of the alluvial plain boundary with the beach barrier or Pleistocene deposits was derived from the CPT analysis. The depths from all these nine sections were linearly interpolated to obtain an estimate of soft soil thickness for the entire research area.

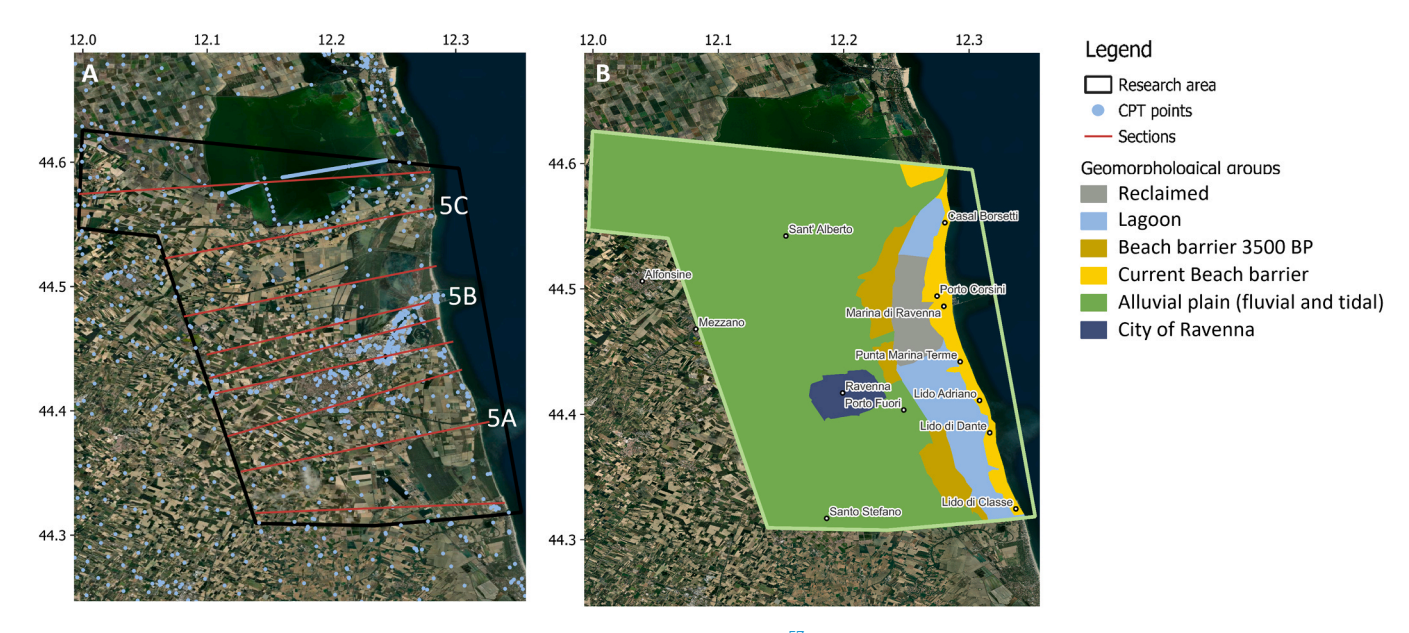
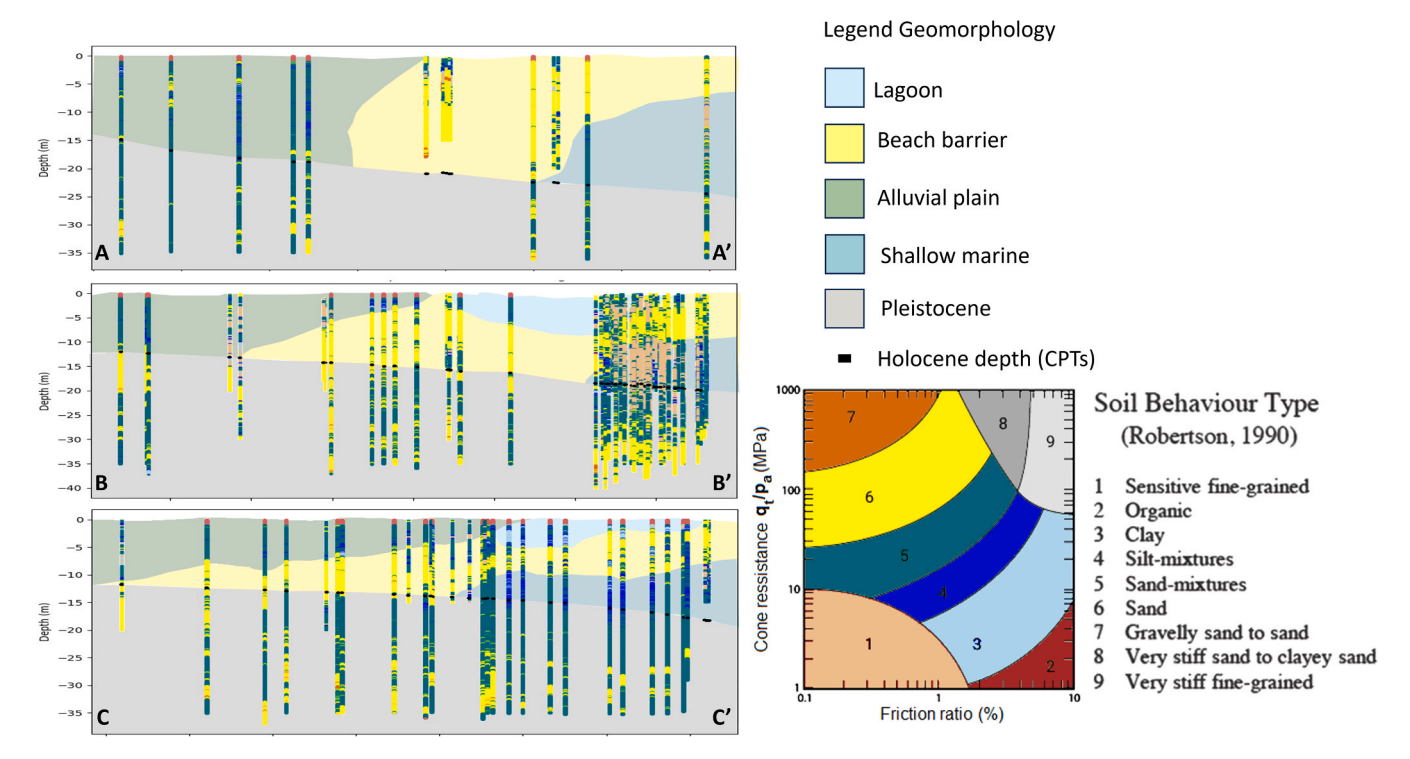


Fig. 4. A: Locations of the CPTs in the research area as provided by the GSSS-ER database. <sup>57</sup> The red lines show the traces of the nine sections developed from CPT data to derive the geomorphological mapping product. B: Subdivision of the area in the different geomorphological groups (see Section 3.6).



**Fig. 5.** An analysis of CPT data along three sections indicated in Fig. 4 with 5 A, 5B, and 5 C. The base of the Holocene sequence is determined for each CPT location from the GSSS-ER map<sup>57</sup> of the Holocene depth. For each CPT location, this border is plotted as a black dot. The black dots thus signify the boundary between Holocene and Pleistocene deposits. Robertson<sup>58</sup> classification, see inset to the right, was used for the interpretation of soil types of the CPT datapoints. The geological interpretation is schematized at the background.

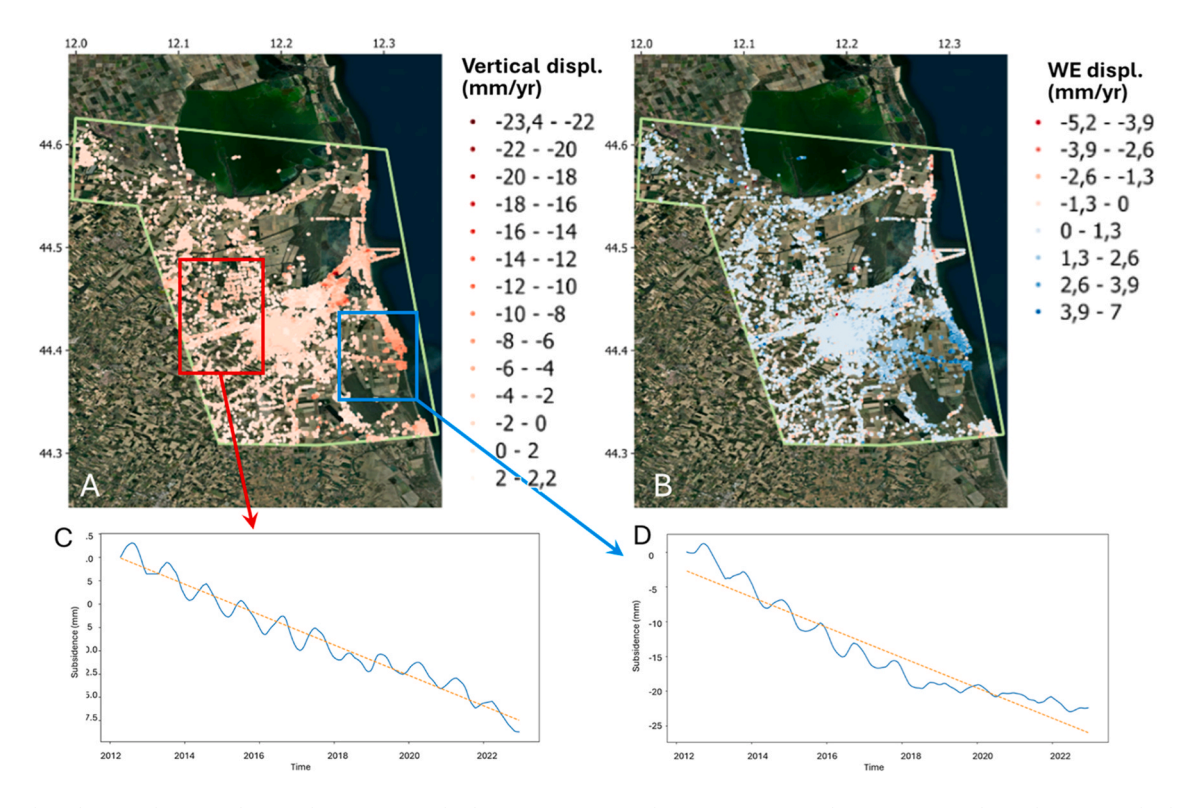


Fig. 6. InSAR data showing the vertical (A) and west-east (B) displacement rates over the 2012–2022 period, prior to resampling. The average displacement time series measured in the two subregions to the east of Ravenna and at coastland in correspondence of the Fiumi Uniti river mouth are provided in (C) and (D), respectively.

### 3.4. Estimate of deep-caused land subsidence

Deep-caused subsidence (caused by processes occurring at depths larger than 500–1000 m) can be associated with natural processes such as sediment consolidation, tectonics, and glacial isostatic adjustment,  $^{15}$ ,  $^{20,74}$  and in some geological contexts with hydrocarbon production. In this study, given the limited area and time period investigated, we consider deep-caused subsidence to be caused solely by hydrocarbon production.

Gas production from a deep gas reservoir is usually associated with pressure decrease within the produced formation causing its compaction and subsequently land subsidence. Previous studies in the coastal plain of the Ravenna area indicate that offshore reservoir compaction resulted in onshore land subsidence around the Fiumi Uniti river mouth. The offshore reservoirs forms a complex field with tens of overlying pools, at depths varying between 3000 and 4000 m.  $^{63,73}$ 

Deep hydrocarbon extraction typically produces a distinct bowlshaped subsidence (e.g. 30,40), more easily detectable in measurements than groundwater withdrawal-related subsidence, due to the former's more localized extent. Therefore, to investigate the contribution of deep subsidence, we fit a subsidence bowl to the InSAR data, rather than modelling land subsidence by gas extraction from this offshore reservoir, since this is a complex procedure requiring the knowledge of gas production from multiple pools composing the reservoir. The subsidence bowl used is the result of estimates from a geomechanical model developed by ENI, the Italian national energy company, with a numerical approach like that of Capasso and Mantica. <sup>18</sup> The model outcome consists of vertical and horizontal displacements at four time-steps (2010, 2015, 2019 and 2027) following historical and forecasted extraction values. Vertical and horizontal movement rates at intermediate timesteps were calculated from the model as average numbers in the periods between the geomechanical model outcomes. We have used the resulting interpolation as a shape proxy by introducing a multiplication factor for the surface movement as an unknown parameter.

### 3.5. InSAR data

We used InSAR data from the Radarsat-2 satellite mission for the surface displacement estimates. The dataset, which had been processed by ENI, consists of the decomposed vertical and horizontal (East-West) displacements on a grid of  $100 \times 100$  m (Fig. 6A and B). They cover the period from April 2012 to December 2022 with 262 images. Note the varying displacement trends across the study area with, as an example, an almost linear trend inland (Fig. 6C) and a significant decrease in

sinking rate along the coastline adjacent to the hydrocarbon reservoir (Fig. 6D).

We applied a temporal filter and a resampling of the data in space and time to reduce the number of data points in the modeling. Resampling in space was employed to prevent overfitting our parameter estimation to certain locations, for example in the Ravenna urban area where the points are relatively dense. We resampled the data based on a resolution of  $500 \times 500$  m, by randomly selecting two points for the vertical and one for the east-west horizontal displacements. This resampling was not applied for the analysis over the coastal strip subarea where we considered the chance of overfitting negligible. Next, the data was resampled over time using the Savitsky-Golay filter with a first order polynomial. Temporal filtering was applied to prevent sampling of outliers when resampling the data in time. The data is resampled to 120 points in time over the modelling period, which reflects approximately one point per month.

# 3.6. Geomorphological interpretation

The general geomorphological environment, perpendicular to the coast, is summarized in Fig. 7. It is based on Amorosi et al., <sup>4</sup> Bondesan et al., <sup>14</sup> Maselli and Trincardi, <sup>44</sup> and on the CPTs analyzed in this study. This cross section shows the subsurface architecture of the geomorphological classes. The positions of the current and the 3500 year BP beach barriers are situated where sand outcrops. The lagoon environment is located in between the outcropping sand and the alluvial plain is more inland.

To determine the spatial distribution of the subsidence potential, we have divided the research area into six sub regions (Fig. 4B). The underlying assumption is that within these groups the subsurface characteristics are similar and hence the subsidence behavior is similar. We used the soil texture map class 'sand' (Fig. 3) to outline the beach barriers. The clayey lagoon is situated between the two sandy barriers. Within the lagoon, we delineated the area that has been reclaimed over the first half of the last century. The alluvial plain is defined as everything inwards from the paleo beach barrier. Within the alluvial plain, the city of Ravenna was attributed with its own class because it has a significantly higher density of buildings, some of them centuries old. The long history of compaction by urban loading makes the subsurface of Ravenna behave stiffer than less heavily urbanized areas. For the alluvial plain, the depth of the beach barrier, as derived from the CPT analysis (Fig. 6), is considered. The thickness of the compaction-prone sediments varies largely in the alluvial plain and thus the subsidence potential varies.

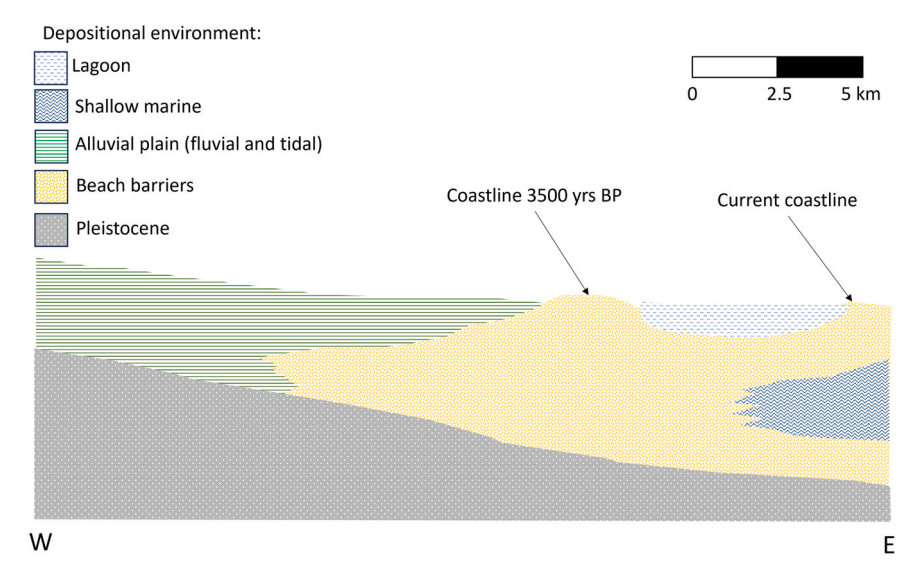


Fig. 7. Schematic profile of the geomorphological setting of the research area, perpendicular to the coast.

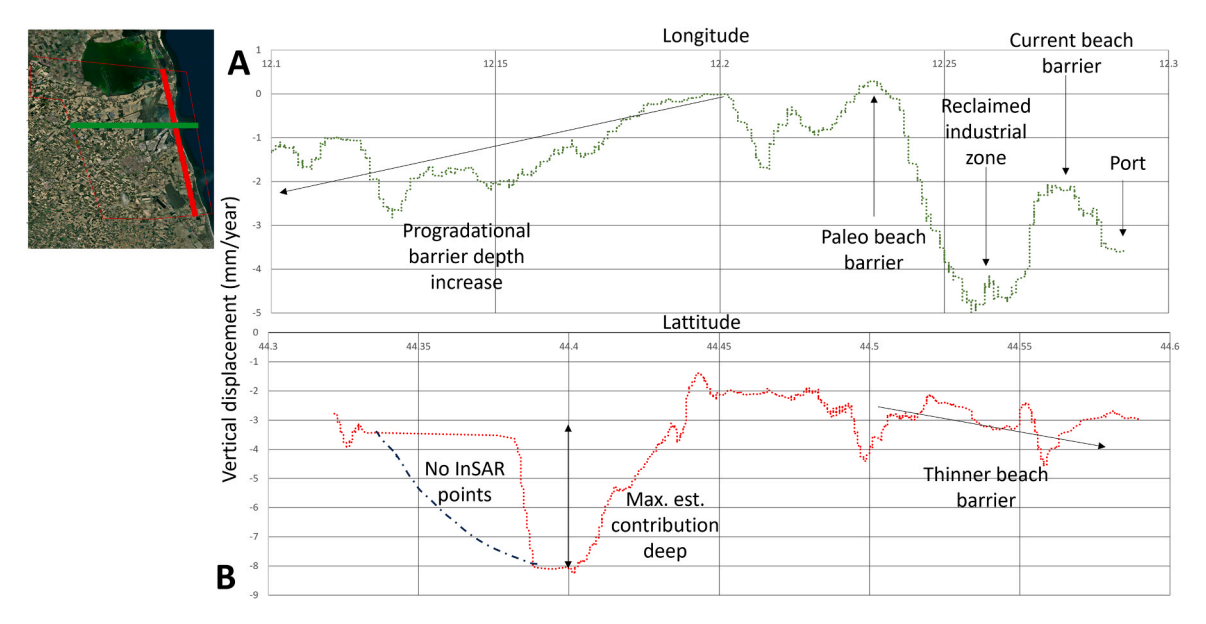


Fig. 8. Moving average of the mean subsidence velocity in mm/year along the two alignments, shown in the inset map. Our own interpretation is added to this. The top profile runs perpendicular to the coastline, north of Ravenna and south of Sant'Alberto. The bottom profile is along the coast, following the thickness of sand according to the soil texture map of GSSS-ER. Because we calculated a moving average along the sections and due to a lack of InSAR points in the southern part of the bottom section, we added a likely interpretation of the displacement variation in the southern part of the section.

# 3.7. Subsidence model

To estimate the total subsidence, we model three subsidence causes: processes related to building load  $(S_b)$ , processes within the shallow subsurface  $(S_s)$ , and processes within the deep subsurface  $(S_d)$ . The total subsidence  $S_{total}$  on each location and at every time step is the sum of all the contributing components:

$$S_{total} = S_b + S_s + S_d \tag{1}$$

# 3.7.1. Building cause

Compaction occurs when pore space reduces and consequently soil particles are pressed together by an effective stress increase or by creep due to the application of a load on the land surface. The rate of compaction due to stress reduces over time as the expulsion of pore water decreases, which is expressed in established empirical logarithmic equations such as the Bjerrum model ( $^{12}$  CUR Centre for Civil Engineering, 1996;  $^{24}, \,^{82}$ ) and the Koppejan model (CUR Centre for Civil Engineering, 1996;  $^{24}$ ).

To calculate the actual stress by building load applied to an area, detailed building information is necessary. Additionally, adjacent structures such as streets, parking spaces and playgrounds could add to the stress imposed on the subsurface. To simplify, we therefore consider the differential building volume from the GHSL as a proxy for the applied stress. We differentiate between dominant industrial or residential buildings per  $100\times100$  m grid. On average industrial buildings have a larger weight and hence induce more stress on the underlying soil.

Eq. (2) shows the relationship applied in this study. It calculates building subsidence ( $S_b$ ) by summing monthly differential subsidence changes, accounting for monthly estimates, interpolated from the GHSL dataset in time, of differential building volume:

$$S_b(t) = -\sum_i C_s \times V_i \times I \times D \times \log\left(\frac{(t - t_i) + 1}{\tau}\right)$$
 (2)

In this equation  $C_s$  is the soil compaction coefficient, specific for each geomorphological class (Fig. 4B).  $V_i$  is the differential building volume at timestep  $t_i$  in years. I is the factor for industrial buildings versus residential buildings. I is set to 1 for residential dominated grid cells and varied (with I > 1) for industrial buildings. The first timestep is 1975,

coinciding with the earliest available building data from the GHSL database. D is a factor to take into account the thickness T of the subsidence-prone sediments in the alluvial plain and is calculated for each individual location as  $D=d\times T$  where the parameter d is a single parameter for the alluvial plain to be optimized. D is set to 1.0 for all geomorphological classes, except the alluvial plain.  $\tau$  is a time constant influencing the rate of subsidence, added for consistency with the Bjerrum functions (e.g.  $^{24}$ ). For this study, we set the value to one month to calculate monthly subsidence increments, aligning with the InSAR observations.

# 3.7.2. Shallow cause

We define shallow causes of subsidence as the processes that take place within the soft soil of the coastal sequence as a result of stress imposed by overlying sedimentary layers. Relatively young, soft finegrained and organic sediments are compaction-prone when stress increases. The alluvial plain, Ravenna city, and the beach barriers are predominantly sandy, exhibiting stiffer behavior than lagoonal clay. Consequently, we assume minimal shallow subsidence contribution from these areas. Our focus is on processes in the geomorphological classes in the coastal zone: reclaimed land, current coast, and lagoon. There are two likely causes for ongoing subsidence in these areas. The first is compaction of the tidal deposits, overlain by the younger coastal deposits (Fig. 7). The weight of the overburden of the younger coastal deposits can result in natural soil compaction, 90 exacerbated by natural shrinkage and oxidation of clay and peat deposits respectively.<sup>81</sup> The second process is compaction of reclaimed land. The clayey lagoon deposits are relatively young, and have been partly reclaimed, recently or in the past. For the reclaimed land, the compaction is likely still ongoing because of the effect of drainage induced stress.<sup>29</sup> The driving forces of the current coast and the lagoon class are the same; we therefore combined these two classes.

Like compaction by building-load, soil compaction is a process that reduces over time. However, on the timescale of this study, the change in compaction rate will be negligible, <sup>81</sup> hence a simple linear model suffices:

$$S_s(t) = -B_s \times \Delta t \tag{3}$$

where  $B_s$  is the natural soil behavior parameter for natural shallow

processes for the reclaimed land and the lagoon and coastal zone., and  $\Delta t$  the time passed since the first time we calculate the subsidence, i.e. 1975.

### 3.7.3. Deep cause

The third subsidence cause is compaction of a gas reservoir. As gas is extracted, reservoir pressure decreases, causing compaction. This reservoir compaction translates to surface subsidence. This process is included in our approach by fitting a subsidence bowl to the InSAR observations with a factor. The displacement bowl is estimated over time, both as a horizontal east-west and a vertical component. To appreciate the uncertainty of the given estimate, we scale the bowl to the outcome with a single factor as:

$$S_d(t) = A * S_{bowl} (4)$$

in which A is the scaling parameter and  $S_{bowl}$  the initial subsidence bowl estimate as simulated by ENI (see Section 3.4). We use a single parameter A for both the horizontal component and the vertical component. Initially A is set to 1.0, assuming that the provided  $S_{bowl}$  is accurate. The scaling parameter can increase or decrease depending on the fit with the InSAR derived subsidence estimates.

# 3.8. Integration into the data assimilation framework

We applied an Ensemble Smoother with Multiple Data Assimilation (ES-MDA, Appendix A) to i) the total research area and ii) the  $\sim$ 5 km wide coastal strip with performance assessment through the chi-square error, absolute error (AE) and average ensemble spread (AES) (Appendix A). The coastal strip includes all InSAR derived subsidence estimates from the geomorphological classes of the current and paleo coast, the lagoon and the reclaimed land (Fig. 4B).

For the total research area, 11 parameters were estimated, of which the prior estimate and standard deviation are given in Table 1. The coastal strip contains the geomorphological classes of the paleo beach

**Table 1** Parameters for the total research area, prior and posterior to the data assimilation procedure. For the final fit, the  $\chi^2$  error has been reduced from 14.36 to 4.93. AE = 0.70 and AES = 0.20. See Appendix A for the definition of the fit metrics.

Parameter	Prior	Posterior	Number of InSAR locations	
Compaction soil parameters, building cause $(C_s)$				
Alluvial plain	3.00	0.65	1643	
	$\pm~0.20$	$\pm 0.06$		
Paleo beach barrier sand	1.50	0.19	58	
	$\pm~0.20$	$\pm 0.20$		
Lagoon	4.50	31.84	135	
	$\pm~0.20$	$\pm 1.43$		
Current beach barrier	4.50	6.22	154	
	$\pm~0.20$	$\pm 0.53$		
Reclaimed land	6.00	7.95	69	
	$\pm~0.20$	$\pm~0.52$		
Ravenna	4.00	3.97	127	
	$\pm~0.20$	$\pm~0.40$		
Natural soil parameter, shallow cause $(B_s)$				
Reclaimed	4.00	4.30	69	
	$\pm~0.10$	$\pm~0.09$		
Lagoon	1.50	1.85	289	
	$\pm~0.10$	$\pm~0.11$		
Other parameters				
Weight depth progradation barrier effect $(d)$	1.00	0.13	1643	
	$\pm 0.10$	$\pm 0.01$		
Industry factor (I)	5.00	2.00	358	
	$\pm \ 0.20$	$\pm~0.07$		
Deep cause model factor (A)	1.00	0.62	2807 (621 locations EW)	
	$\pm \ 0.10$	$\pm~0.05$		

barrier, the lagoon, reclaimed land and the current beach barrier. For the coastal strip 8 parameters were included (Table 2): it does not include the geomorphological class of the city of Ravenna and the alluvial plain, nor the effect of thickness

The values of the ensemble parameters were determined from a normal distribution of the parameters with the error as standard deviation. Since there are no previous studies in the area using similar analytical subsidence models, the initial values were chosen so that the subsidence effect of each process is in the order of magnitude of the subsidence from the InSAR-derived estimates.

The data contain 120 timesteps over a period of 10 years. For the complete research area, a total number of 2186 locations were included for the vertical movement and 621 for the horizontal west-east movement. Tables 1 and 2 indicate how many of the InSAR locations are affected by a certain parameter (e.g. the locations in the alluvial plain are not affected by parameters of the lagoon). The error to these data points was set at a standard deviation of 5 mm. This error takes into account the measurement errors and the model errors. We used eight assimilation steps of 500 ensemble members to optimize the parameter values. The reduction factor q in Eq. A3 of the Appendix A was set at 2/3 and the inflation factor  $\gamma$  (eq. A4 in Appendix A) at 1.9 for the total research area and 1.8 for the coastal zone. These values were determined by trial and error, and they form a trade-off between accuracy of the models, final spread, stability and running time.

### 4. Results

The results section is divided into three parts. The first part presents a simple analysis of the InSAR data, enabling the identification of the important factors to include in the modeling. The second part shows the data assimilation analysis of the entire research area. This is followed by the analysis of the coastal strip to highlight some important results in more detail.

# 4.1. InSAR analysis

Fig. 8 shows the moving average of the mean vertical displacement rates as provided by InSAR on alignments perpendicular to and along the coast. The pattern on the trace perpendicular to the coast is based on the InSAR points on a west-east transect located between the city of Ravenna and Sant'Alberto town. The pattern on the trace along the coast includes all InSAR points in the geomorphological class of the current beach barrier (Fig. 4B).

Perpendicular to the coastline, the higher subsidence rates in the easternmost parts correspond to the values in the seaward side of the Port of Ravenna. The subsidence rates reduce towards the current beach barrier. More inland and westward, the largest subsidence rates are observed. These rates correspond to the lagoonal and partly reclaimed,

**Table 2** Parameters for the coastal area, prior and posterior to the data assimilation procedure. For the final fit, the  $\chi^2$  error has been reduced from 9.15 to 8.53. Here, AE=0.96 and AES=0.48. See appendix A for the definition of the fit metrics.

Parameter	Prior	Posterior		
Compaction soil parameters, building cause( $C_s$ )				
Paleo beach barrier sand	$1.50\pm0.20$	$0.31\pm0.03$		
Lagoon	$4.50\pm0.20$	$3.27\pm0.11$		
Current beach barrier	$4.50\pm0.20$	$0.85 \pm 0.04$		
Reclaimed land	$6.00 \pm 0.20$	$6.25\pm0.20$		
Natural soil parameters, Shallow cause (B <sub>s</sub> )				
Reclaimed	$4.00 \pm 0.10$	$4.34 \pm 0.03$		
Lagoon	$1.50\pm0.10$	$2.12\pm0.03$		
Other parameters				
Industry factor (I)	$5.00 \pm 0.20$	$8.71 \pm 0.22$		
Deep cause model factor (A)	$1.00\pm0.10$	$0.67 \pm 0.01$		

heavily industrialized zone. Subsidence rates diminish further westward towards the paleo beach barrier. Moving further to the west, there is a gradual increase in subsidence rates, in agreement with the increasing thickness of the alluvial plain.

Along the coastline, from south to north, there is a subsidence bowlshape visible in the southern portion in correspondence of the offshore gas extraction. North of this subsidence bowl, a more gradual increase in subsidence rates is observed northwards. This corresponds to the geomorphological thinning of the current beach barrier and the increase in thickness of the tidal deposits underneath it (Fig. 4B).

Fig. 9 provides for the area of Ravenna a first analysis of the relation between buildings and the subsidence rate by plotting the average vertical subsidence rate over the period 2012–2022 versus the added building volume for each  $100\times100$  m grid from 1990 to 2020. A linear trendline is added to make this relation clearer. It shows that adding more building volume results, on average, in more subsidence. Since building age and (sub)surface properties are not taken into account, outliers are to be expected.

Both the east-west and north-south sections suggest that geomorphological structures are a key factor for subsidence rates. The thickness of subsidence prone sediments, and the geomorphological classes, all correlate with varying subsidence rates. The InSAR analysis of these sections therefore underscores the critical role of current and historical land use and the subsurface geology in shaping current subsidence rates. Also, anthropogenic influence on this pattern should not be diminished; heavy industrialization and gas extraction correlate with increased subsidence rates. Both sections of Figure show variations, besides the patterns and processes indicated in the figure. As the plotted data is the result of a moving average of an area with a width  $> 10 \, \mathrm{km}$ , these variations are either the result of spatial variability in the area (i.e. variation in urbanization degree) or an indication of the uncertainty of the InSAR data.

We can derive from Figs. 8 and 9 the clear correlation between the three key subsidence causes and the observed subsidence. The loading of buildings, especially industrial ones, correlates with increased subsidence rates. Additionally, geomorphology plays a role in subsidence rates. For example, the paleo coastal barrier correlates with low subsidence rates; the rates increase land inwards, correlating with the thickness of the alluvial plain. Additionally, we observe that within the influence range of gas extraction a subsidence bowl is visible.

### 4.2. Optimization in the entire research area

In the optimization procedure of the entire research area, 11 parameters are considered. Table 1 shows the prior estimates and the posterior best fit of these parameters.

From Table 1 we observe that the largest building-related subsidence  $(C_s)$  is on lagoonal deposits, followed by the reclaimed area and the current coast. The slowest subsidence rates correspond to the paleo beach barrier, followed by the alluvial plain deposits. Four of these classes have additional parameters related to shallow subsidence. The shallow cause  $(C_B)$  influences the reclaimed area, the combined lagoon and current beach barrier. The alluvial plain includes a parameter for the effect of the thickness of the compaction prone sediments (related to the depth of the buried inland foot of the beach barrier) (d). Due to these additional parameters that differ per geomorphological class,  $C_s$  (compaction soil parameter for building related subsidence) is not the only indicator of the shallow subsidence potential.

Fig. 10 presents the relative contribution of the different processes to the total subsidence at random locations. Both the total subsidence and the relative contribution of the different processes vary in the study area. The effect of the deep cause diminishes towards the northwest. The shallow cause  $(B_s)$  is present in the reclaimed, lagoon, and current coastal zone. The shallow cause is generally dominant. Note that the locations are chosen randomly and that subsidence varies per individual location

Figs. 11 and 12 plot the average modelled subsidence, the InSAR-derived displacement estimates, and the difference between these two for the vertical and for the horizontal east-west component respectively. Fig. 13 plots the average vertical contribution for the three modelled processes. For the vertical component (Fig. 11), the largest subsidence rates are in the reclaimed area, followed by the southeast part along the coast and the lagoon area. In the alluvial plain the subsidence rates are on average the lowest. In the alluvial plain we observe an increase in subsidence towards the west. The locations of areas with the largest differences between model and observations are also identified in Fig. 11C and their potential causes are outlined in the discussion section. Concerning the horizontal movements, Fig. 12 shows that the largest contribution provided by the model is located more to the west compared to the InSAR derived subsidence estimates. Along the coast the modelled displacement underestimates the InSAR measurements.

We have selected six locations (Fig. 10) that are representative of the total subsidence by the three modelled processes, Fig. 14 shows the fit of

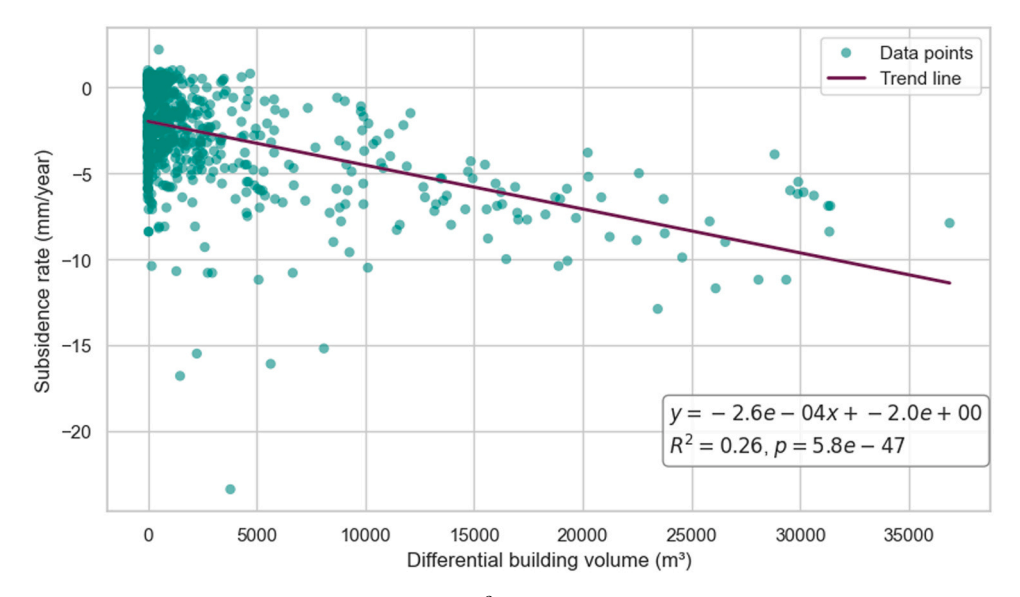
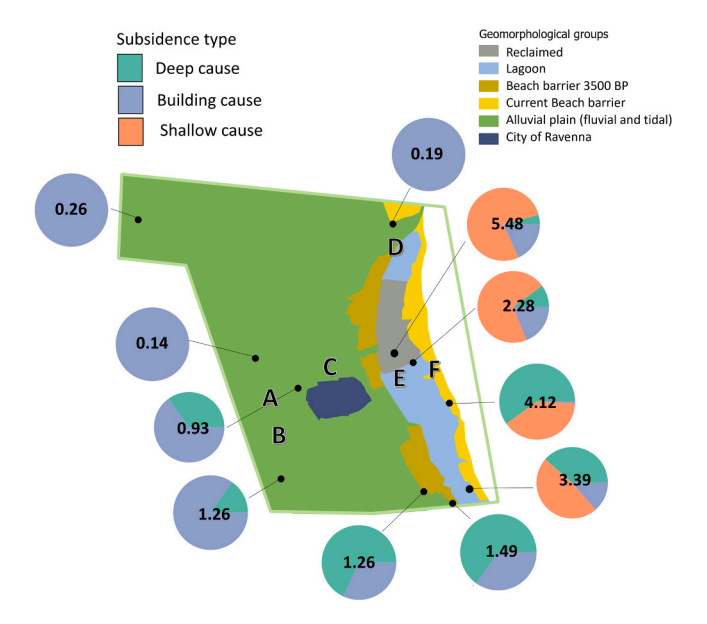


Fig. 9. Subsidence rate in mm/year versus the differential building volume (m³) from 1995 to 2020 for the InSAR points that fall within the geomorphological class of the city of Ravenna (Fig. 4B). Subsurface properties, building age and building purpose are not taken into account, therefore outliers are likely to occur.



**Fig. 10.** Relative contribution of the different subsidence processes at random locations throughout the area. The total subsidence rate is provided by the number in mm/year. Note that the amount of building related subsidence depends on the amount of differential building volume and, for the alluvial plain, on the depth of the progradational beach barrier as well. The letters on the figure correspond to the locations whose displacement time series are plotted in Fig. 14.

the modelled subsidence to the InSAR-derived subsidence data. In all these plots the spread in vertical displacements has been reduced with data assimilation. Location A, B and D show a non-linear behavior over time for the modelled subsidence. For locations B and D, this is (partially) correlated with the onset of a new logarithmic trend each year. This is a result of our assumption to set the change in differential building volume contribution at the start of each year, instigating additional compaction by loading. The locations C, E, and F show a more linear trend. The total subsidence over time varies largely per location.

Fig. 13 shows the estimates per assimilation step for individual locations; Fig. 15 shows the parameter value estimate per assimilation step, for four different parameters with the progressive assimilation steps. No significant correlations were found between the parameters investigating the entire research area.

# 4.3. Coastal strip

We made an assimilation for subsidence on the coastal strip, including the InSAR points in the areas of the geomorphological classes: lagoon, current beach barrier, paleo beach barrier, and the reclaimed land. The analysis includes the eight different parameters that model natural soil compaction ( $B_s$ ), building-related compaction ( $C_s$ ) and compaction due to gas extraction (A).

Table 2 presents the prior and posterior parameter estimates in the coastal strip. The paleo beach barrier exhibits the slowest  $C_s$  subsidence rates. The largest  $C_s$  subsidence rates are associated with the reclaimed area, followed by the lagoon area, and lastly the current beach barrier. The natural soil compaction,  $B_s$ , in the reclaimed area is larger than in the lagoon area. These outcomes are similar to the results for the entire research area.

Fig. 16 shows the modelled subsidence rates for the coastal area, the InSAR-derived estimates, and the difference between the two. The largest differences are found at some specific points in the industrial reclaimed zone. Along the coast in the southern part, in correspondence of the influence zone of hydrocarbon production, the subsidence is generally underestimated. Conversely, it is often overestimated more inland, except for some points in the industrial reclaimed zone.

In contrast to the total research area, there is a significant correlation between two parameters for the coastal strip. Fig. 17 plots the correlation matrix for all parameters of the coastal area. The strongest correlation is the one between the industry factor and the lagoon  $C_s$ parameter. An increase in the effect of industry reduces the effect of the natural soil parameters of the lagoon. Indeed, as the lagoon has abundant industry, and consequently, the distributions of the two largely overlap, the effect of an increase in one of the parameters can be compensated by a decrease in the other. This correlation is demonstrated in Fig. 18A for the progression of assimilation steps. For each assimilation step, the parameter spread of the lagoon is plotted against the factor for industry. There is a linear correlation visible, that strengthens with the data assimilation steps. An increase in the industry factor would lead to a decrease in the lagoonal natural soil parameter. Fig. 18B shows the lagoon natural soil parameter versus the current coast compaction soil parameter. In this case, there is no strong correlation between the two parameters in all of the assimilation steps.

# 5. Discussion

The analysis of land subsidence in the Ravenna area over the decade 2012–2022 reveals complex spatial and temporal patterns driven by

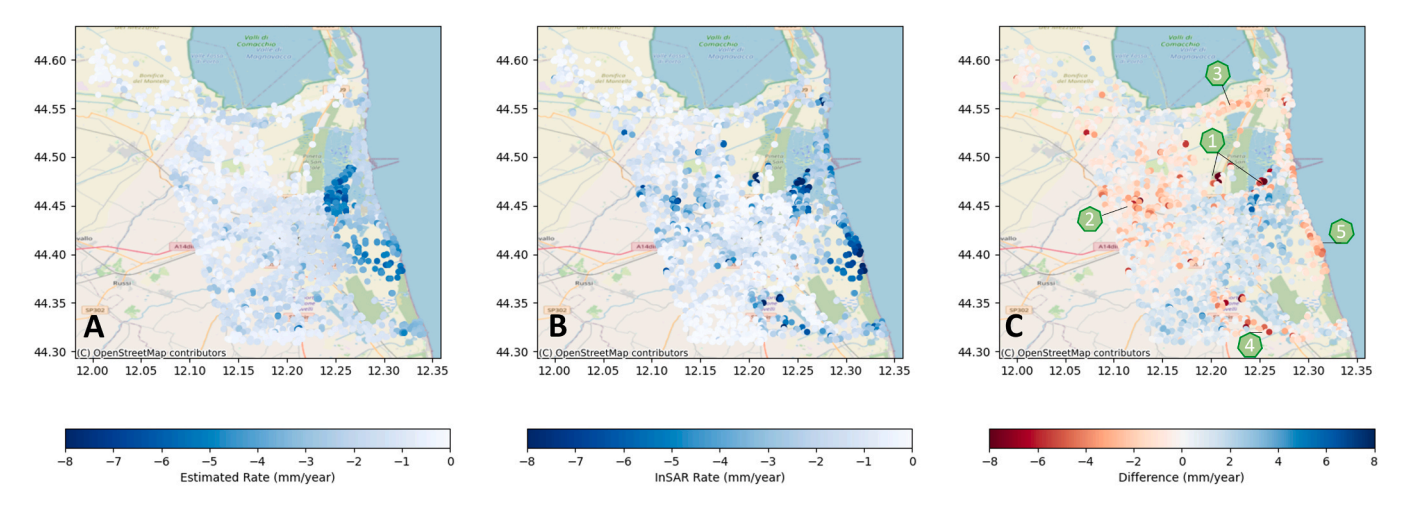


Fig. 11. A: Simulated estimate of land subsidence per location. B: InSAR vertical component. C: Difference between the model estimate and the InSAR data. The difference is negative when the InSAR data shows more subsidence compared to the optimal model estimate and positive when the estimate is larger than the InSAR data.

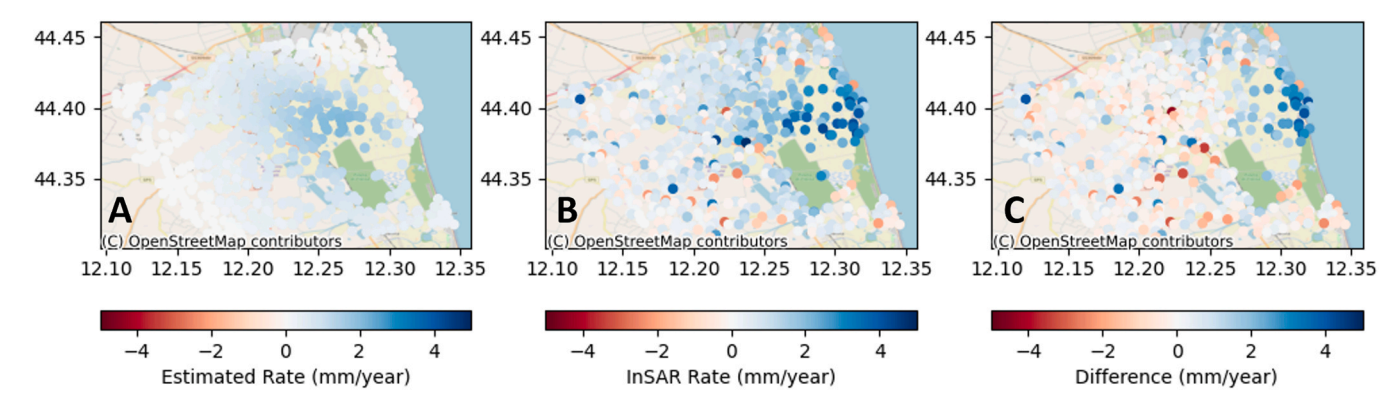


Fig. 12. Horizontal west-east movements over the study area with positive and negative values indicating eastward and westward direction, respectively. Only the datapoints that fall within the range of motion according to the geomechanical model are included. A: Simulated estimate. B: InSAR horizontal east-west component. C: Difference between the InSAR data and the model estimate. The difference is positive when the InSAR data shows a larger eastward displacement compared to the optimal model estimate.

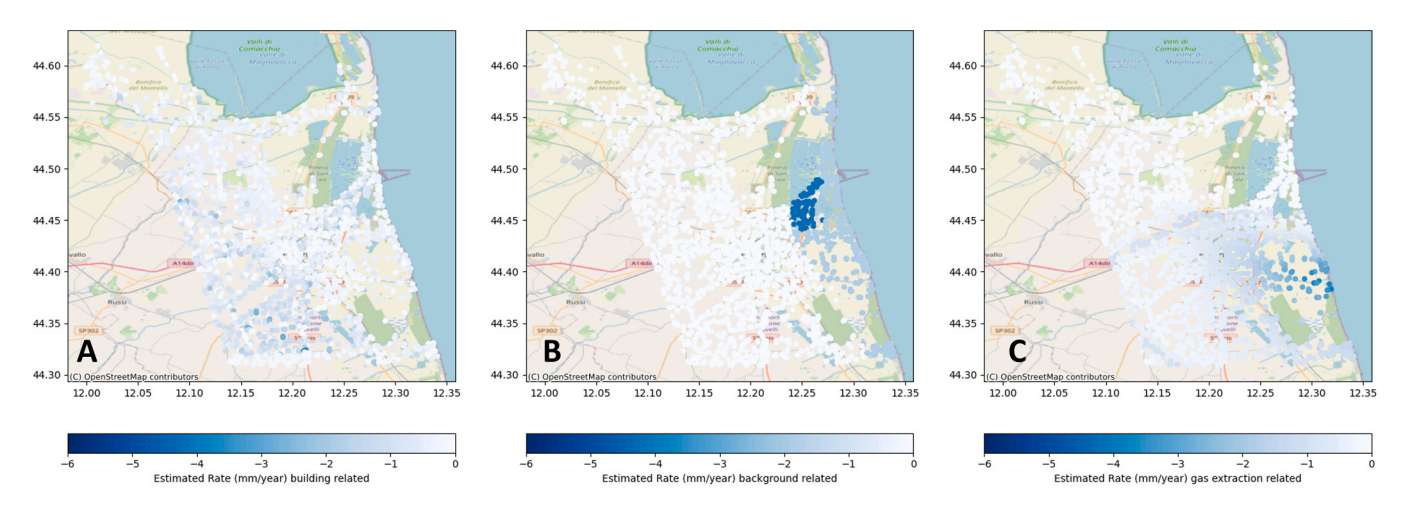


Fig. 13. Relative average contribution of the difference subsidence causes, based on the optimized model estimate. A: Contributions of the building cause. B: Contributions of the shallow cause. C: Contributions of the deep cause.

various geological and anthropogenic factors. In this section, we discuss the various subsidence processes, the difference between the modelled and observed subsidence and the data assimilation analysis, including the parameter estimates, variations and correlations. In addition, we consider the limitations and implications of these findings.

### 5.1. Subsidence processes

We have identified three main subsidence processes: (i) the building cause, (ii) the shallow cause and (iii) the deep cause. Fig. 10 shows that the different processes affect the research area differently. We will discuss the identified processes and the differences between modelled and observed subsidence.

Fitting a limited number of parameters (11) to a large dataset (over 1000 points with 120 time-steps each) leads to averaging the behavior of different processes. As a consequence, differences between model and data will occur. These differences are crucial for understanding the subsidence processes, because they may give hints to the limitations of the models. Such limitations can be the unaccounted natural variation in the system, or the lack of incorporation of additional subsidence causes in the models. The most significant discrepancies between modelled results and InSAR-derived estimates are indicated in Fig. 14C and will be discussed here.

# 5.1.1. Building cause

The built-up environment significantly affects land subsidence rates.

This process is non-linear with time (Eq. (2)) and depends on the differential building volume over time (Fig. 14). An increase in building volume leads to an increase in subsidence (Fig. 9). This was also noted by Fiaschi et al.<sup>27</sup> and Grassi et al.,<sup>37</sup> who did an InSAR analysis of the Ravenna region and related this to land use and geographical building data. The nature of buildings is also relevant, with industrial buildings causing subsidence rates approximately two times faster than residential buildings (Table 1). This effect is even more pronounced in reclaimed areas, where compaction due to the weight of industrial structures causes the largest subsidence rates (Figs. 11 and 12). Fiaschi et al.<sup>27</sup> also indicated that the reclaimed industrial area belongs to the fastest subsidence regions in the Ravenna region.

The largest differences between our modelled subsidence and the InSAR data are also in the reclaimed industrialized area (point 1 in Fig. 11C). This is likely due to the nature of the industry present. Some of it consists of storage of large gravel, sand and calcareous rock piles, combined with large silos to process sands, rocks and gravel (Fig. 19). The grid-based decomposed InSAR-derived estimates show subsidence rates up to 23 mm/year over the period 2012–2022 for the location of Fig. 19. Subsidence rates derived from points on top of individual buildings are therefore likely even higher.

This exemplifies the generalization in our approach, where we do not account for the exact nature and size of buildings but provide a generalized overview on a scale of  $100 \times 100$  m. If we compare the coastal strip results with the results for the entire research area, we observe the effect of this generalization. Relatively heavy industry takes place in the

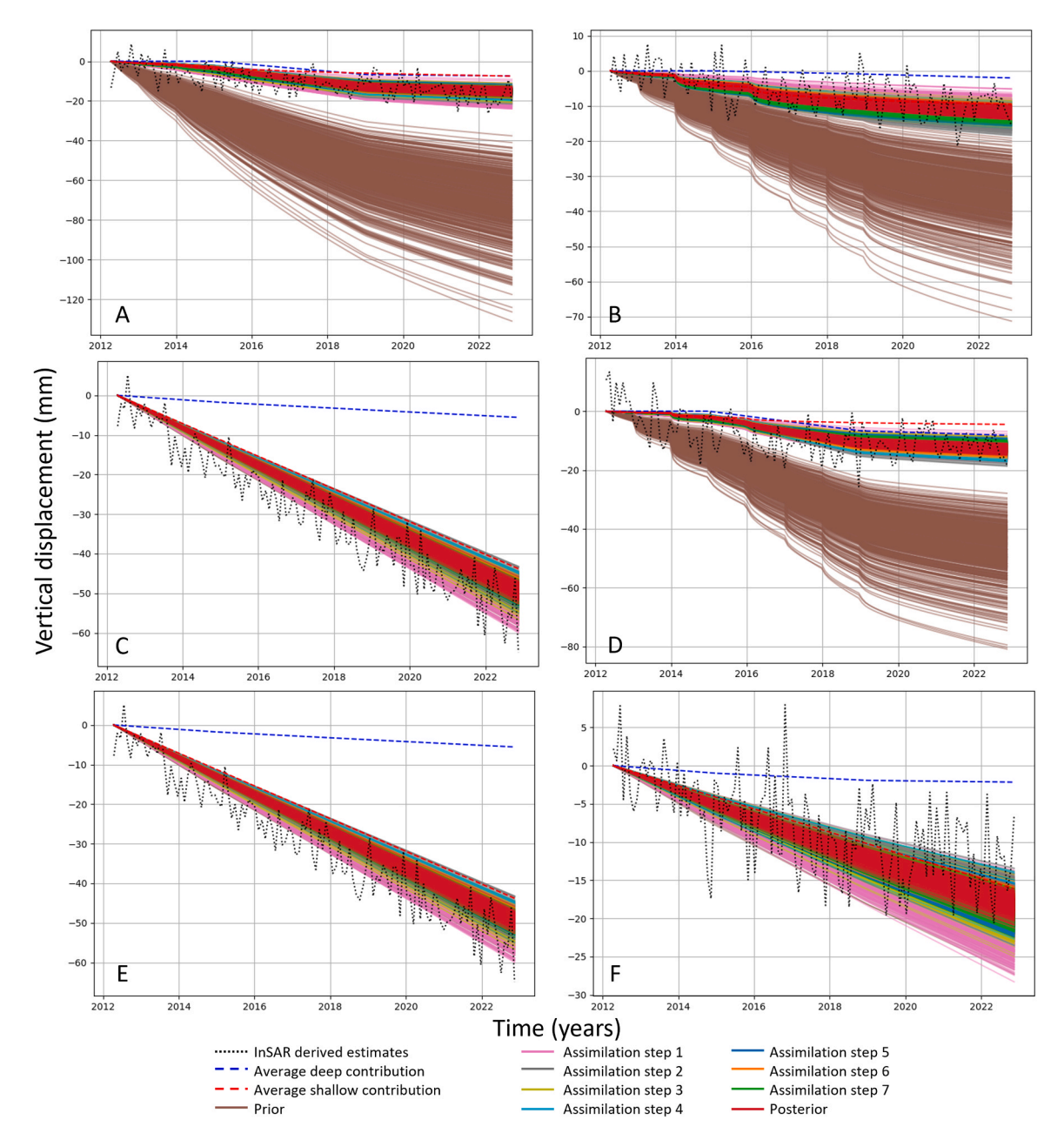


Fig. 14. Timeseries of vertical displacements for the six representative locations identified in Fig. 10 with the letters A, B, C, D, E and F. Each plot shows the prior estimate, and the ensemble estimates for each assimilation step. The processed InSAR data with 5 mm standard deviation random noise is plotted and the average shallow (soil compaction and building compaction) and deep contribution are plotted for the final assimilation step in red and blue respectively. Notice that the range of the vertical axis varies among the sub-plots.

industrialized reclaimed area. If the research area is smaller, the relative importance of datapoints in this area increases. Therefore, the factor by which industry increases building-related subsidence increases from  $\sim\!\!2$  to  $\sim\!\!8$ . These values indicate that industry contributes significantly more to subsidence along the coastal strip, especially in the reclaimed zone. Determining the industry factor over the entire research area averages out the type of industry having a different effect on the total subsidence.

Factors such as foundation type, pre-loading of the surface, building location, and structural characteristics should be further examined to be able to predict subsidence due to industrialization and urbanization more precisely. Other studies have already shown that both on a scale of several kilometers (e.g. <sup>28,81</sup>) and tens of meters<sup>79</sup> the influence of the soil or geomorphological characteristics is significant. Besides detailed data on buildings, the subsurface characteristics are therefore essential to be able to understand and predict subsidence. Results of the current

study should be interpreted as more general behavior, on the scale of the different geomorphological classes. Yet, it should be kept in mind that these differences contribute to the final error of the parameter estimates (Tables 1 and 2).

# 5.1.2. Shallow cause

We regard the shallow cause as a combination of compaction and creep by the stresses exerted on sediments by drainage and overburden weight of overlying deposits. The cause also includes potential shrinkage of clay and oxidation of organic-rich deposits and peat. Regarding spatial variation in the shallow cause, the coastal subsurface architecture plays a pivotal role. The subsurface schematization of Figs. 5 and 7 indicates that shallow tidal deposits underlie the current coast and lagoonal system. There, we observe the fastest soil compaction rates. The relatively young lagoon and barrier sediments are exerting stress to

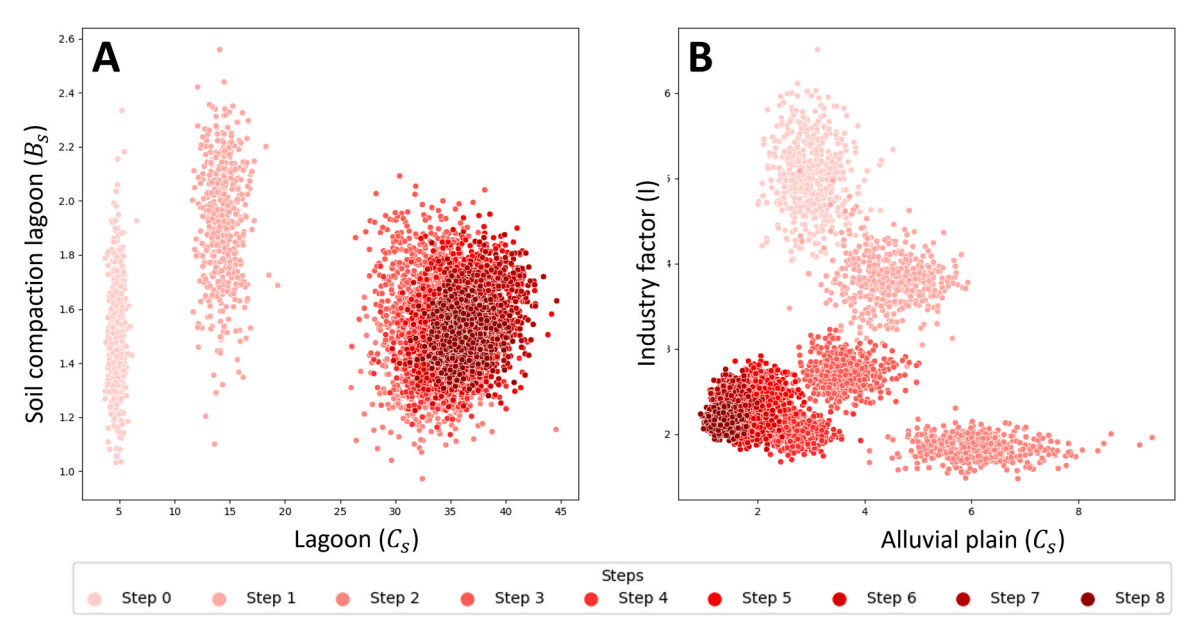


Fig. 15. A: Correlation between the parameters "lagoon compaction soil parameters related to building load" versus "lagoon natural soil parameter" for each assimilation step. B: Correlation between the parameters "alluvial plain compaction soil parameters" versus "industry factor". For both plots, the spread in parameters reduces with each assimilation step, though significantly stronger for the right plot. There is no clear correlation between the parameters. Note that the correlations are for the scatterers per step, and not between the steps.

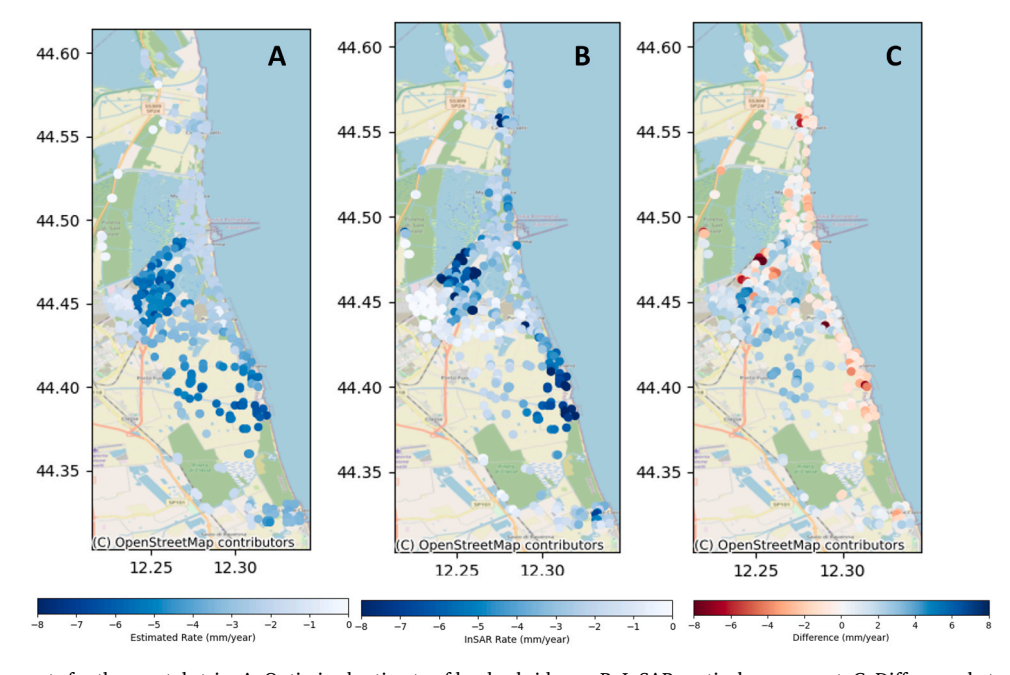


Fig. 16. Vertical movements for the coastal strip. A: Optimized estimate of land subsidence. B: InSAR vertical component. C: Difference between the model estimate and the InSAR data. The difference is defined as negative when the InSAR data shows more subsidence compared to the optimal model estimate and positive when the model estimate is larger than the InSAR data.

the underlying tidal deposits. This drives the soil compaction, until creep rates diminish.

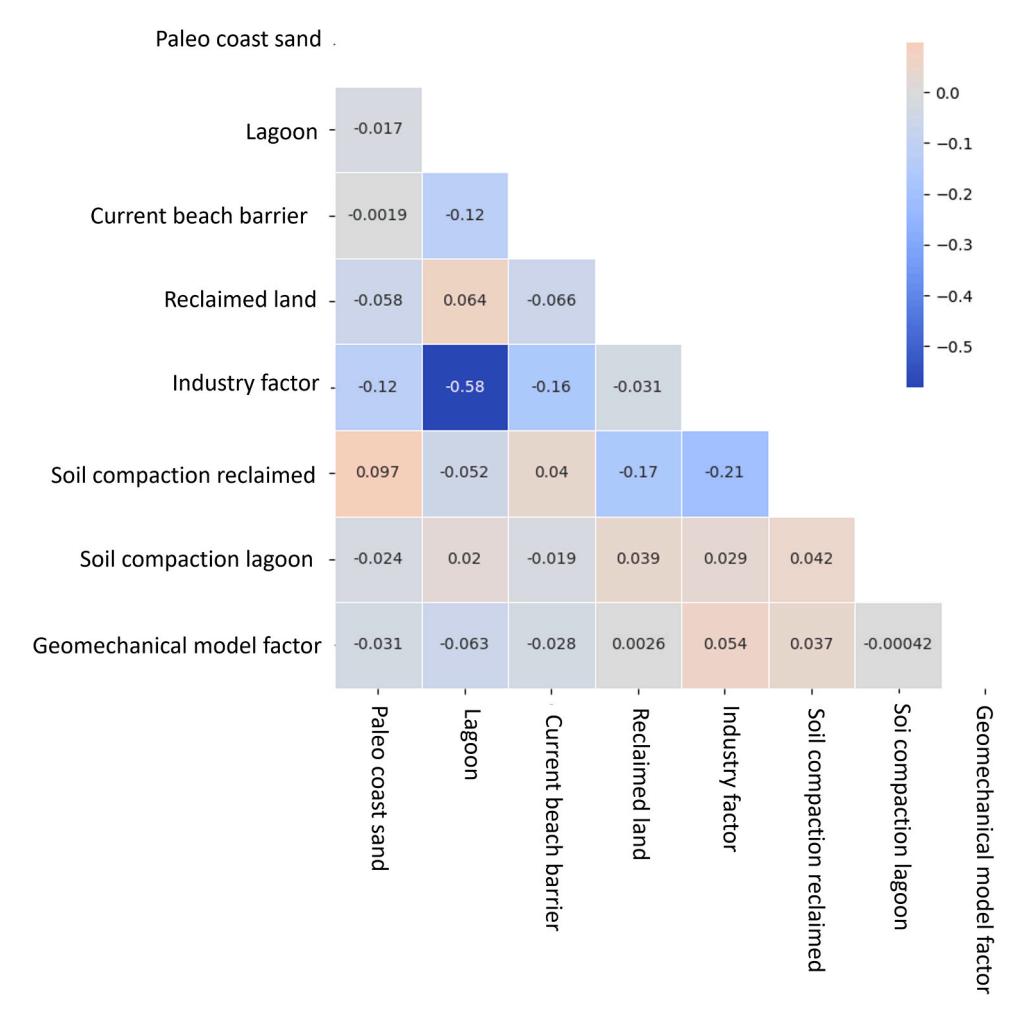
A similar process has been observed in the Netherlands. There, a beach barrier with underlying clayey tidal deposits is gradually compacting by the overburden weight of the beach barrier-complex, locally lowering its topography.  $^{84}$ 

The compaction of deeper soil layers that we observe is not the direct result of human interference, but is caused by indirect interference over the centuries. In a pristine coastal setting, soil compaction would be compensated by sedimentation, because it provides accommodation space. The lagoon and the current beach barrier were formed by

increased sedimentation during the rise of classic civilizations. The present influx of sediments into the system has been reduced by human interferences over the past few decades, by urbanization, reclamation and canalization. Therefore, the coastal area of Ravenna does not receive sufficient sediments anymore to compensate for soil compaction. Sediment starvation of subsiding coastal areas has been observed around the world.  $^{69,87,90}$ 

# 5.1.3. Deep cause

The InSAR measurements point out how land subsidence affecting the coastal zone in front of the offshore gas reservoir significantly



 $\textbf{Fig. 17.} \ \ \textbf{Correlation matrix for the coastal strip analysis of all parameters.}$ 

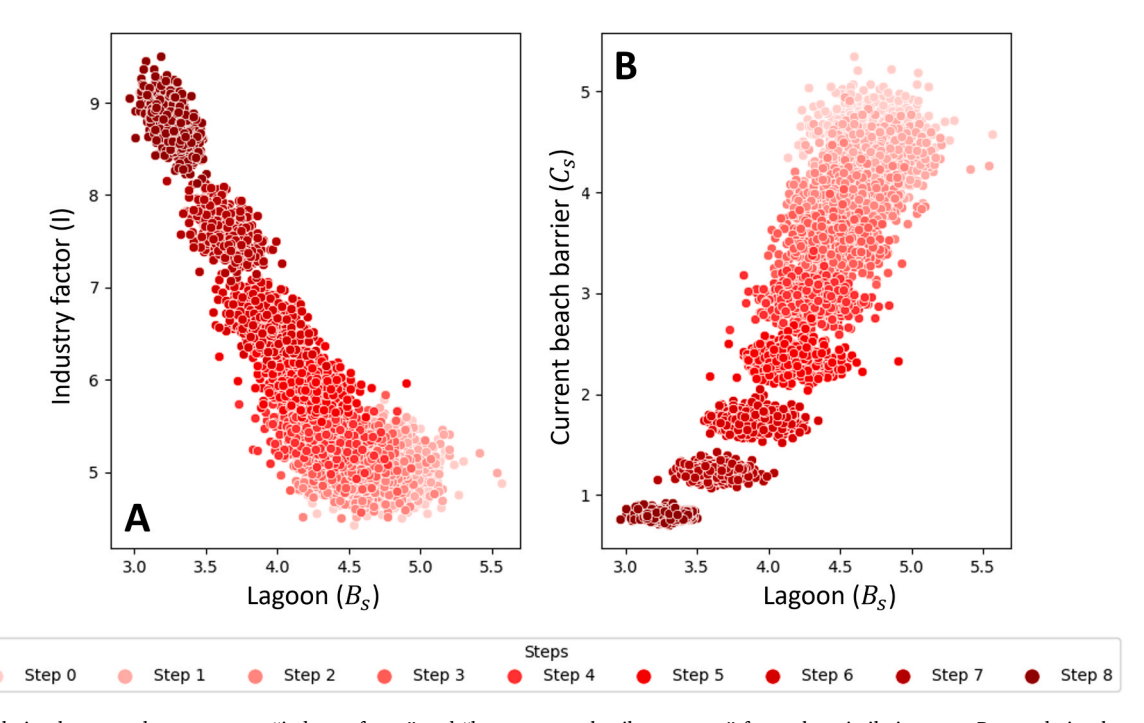


Fig. 18. A: correlation between the parameters "industry factor" and "lagoon natural soil parameter" for each assimilation step. B: correlation between the parameters "compaction soil parameter of the current beach barrier" and "lagoon natural soil parameter" for each assimilation step. Note that the correlations are for the scatterers per step, and not between the steps.





Fig. 19. Industry at the locations where the fastest subsidence rates are identified. GPS coordinates: latitude 44,473609° N, longitude 12,249646° E. Photos taken by Manon Verberne.

decreased over the investigated period (Fig. 6D). Nonetheless, the spatial extent of the subsidence bowl related to hydrocarbon production is evident from the vertical and horizontal east-west movements shown in the decomposed time-averaged InSAR data (Figs. 11 to 13). Surface movements due to gas extraction have a clear horizontal component at the edge of the subsidence bowl. This can be utilized for our analysis, since it indicates the quality of the fit of the modelled subsidence to the InSAR-derived estimates with limited influence of the shallow processes for the horizontal movement.

The east-west movement fit (Fig. 12) shows that the modelled largest horizontal movement is more inland than the InSAR-derived estimates suggest. The observations from the horizontal movements agree with those for the vertical movements (Fig. 11). Along the coast, the vertical movements are underestimated (location 5 in Fig. 11C), while they are overestimated further inland. This suggests that the shape of the modeled subsidence bowl is too wide.

The optimized factor of influence (parameter A) is approximately 0.62. This indicates the InSAR-derived subsidence is about 38 % less than the subsidence from the subsidence bowl prior to parameter optimization. This should be put into the perspective of the bowl shape, as can be clarified by comparing the fits of the subsidence bowl for the entire research area and for the coastal strip. The factor A for the subsidence bowl is slightly larger when only optimized for the coastal strip ( $\sim$ 0.67). In this case, the extent of the area is smaller, inherently not including the effect further away from the center of the bowl. The total modeled subsidence therefore can increase along the coastal strip without having to fit observation data further away from the center of the bowl.

Given these results, the modeled subsidence bowl due to the deep cause appears to be wider and less steep than would fit with the observed subsidence. This often occurs in similar studies globally. Examples are the Lacq gas field in France<sup>64</sup> and the Groningen gas field in the Netherlands.<sup>76</sup> A possible strategy to align the shape of the subsidence bowl would be to include a rigid basement in the modelling of the bowl.<sup>76,75</sup> Other options to obtain a narrower and steeper bowl are anisotropic elastic parameters,<sup>39</sup> an elastic profile with increasing stiffness with depth<sup>30</sup> or a visco-elasto-plastic constitutive model<sup>36</sup>

### 5.1.4. Other processes

The difference between the modelled subsidence and the InSARderived estimates leads us to identify several additional subsidence processes, related to groundwater dynamics, drainage, onshore gas extraction and potential deep natural subsidence causes.

Even though groundwater dynamics are not implemented in our modelling, land subsidence related to groundwater level lowering and withdrawal could explain (partially) the differences between the modelled subsidence and the InSAR-derived estimates. Human-induced groundwater effects can be present due to shallow groundwater drainage and groundwater withdrawal from the confined aquifer

system.

The area northwest of Ravenna (location 2 in Fig. 11C) shows a relatively large error between modelled subsidence and InSAR data. This area is known for large agricultural farms, especially fruit production. Historically, this area has experienced significant groundwater extraction. <sup>10</sup> Although major groundwater extraction no longer occurs, groundwater may still be extracted to some extent for agricultural purposes. This can lead to increased subsidence, which is not included in our modeling approach. The piezometric network managed by the Environmental Agency of the Emilia-Romagna Region <sup>57</sup> does not show significant lowering of the aquifer pressure over the last two decades. However, some delayed effects from the past occurrence, i.e. a delayed propagation of the pressure decline within the aquitards and/or creep deformation, could impact the area still nowadays.

Another factor not considered in our model is drainage. Areas below mean sea level, such as the northernmost (location 3 in Fig. 11C) and southernmost (location 4 in Fig. 11C) parts of the study area, require drainage to prevent the area from inundating (e.g. 67). Not accounting for this can result in an underestimation of subsidence in these regions. Artificial lowering of phreatic groundwater levels is a major cause of land subsidence in the coastal plain of the Netherlands, where large parts of the country lie below the mean sea level (e.g. 41,81). It is likely not coincidental that the areas below the mean sea level show a relatively large difference between modelled subsidence and InSAR-derived estimates.

In the northeast of Sant'Alberto and north of Casal Borsetti our model underestimates subsidence (location 3 in Fig. 11). As not only a difference in vertical subsidence rates, but also some horizontal movement towards the west is observed (Fig. 6), it is possible that a deep subsidence cause influences this part of the region as gas was produced from an onshore reservoir nearby (e.g.; 8,63,71). Though production has largely ceased, 66 there could still be a small effect present, for instance due to ongoing pressure equilibration between the gas reservoir and the connected aquifer. Earlier accounts to model the surface movement here resulted in rates of maximum of 1.3 mm/year. 66

Finally, we note that other deep processes possibly causing land subsidence in the study area, such as tectonics, glacial isostatic adjustment, and consolidation of the Quaternary deposits, have been neglected in this study. Their contributions would be in the order of 1 mm/year at most,  $^{15,20}$  and may explain a portion of the modelling error.

These discrepancies underline the limitations of the current model setup, particularly the exclusion of groundwater effects, detailed industrial structure types, and dynamic drainage behavior. Future work should consider integrating these processes to improve subsidence attribution. The available data is insufficient to include these additional processes in the modeling. However, considering the differences between the modelled subsidence and the InSAR-derived subsidence records, we estimate the processes related to the groundwater and aquifer drainage to contribute at most 2–3 mm/year in some locations, and the

unmodelled deep cause to contribute at most 1 mm/year in the northern part of the study area. The order of magnitude of the drainage and groundwater related values is in line with the rates reported by Antonellini et al. $^7$ 

### 5.2. Data assimilation

The modelled subsidence has been optimized through a data assimilation approach. This approach renders careful interpretation, related to the parameter constraints, the correlation between parameters and the inflation factor used in the data assimilation process. These important points of this analysis are discussed here.

## 5.2.1. Parameter constraints

The data assimilation analysis, which constrains 11 parameters, reveals the complex dynamics driving land subsidence across the study area (Table 1). In ES-MDA the error of the total dataset is minimized by optimizing the parameter values. The constraining power varies among parameters, largely influenced by the number of locations they affect. Parameters that affect fewer data points have a smaller impact on the total error, therefore their final estimate may have a larger uncertainty. Conversely, parameters influencing more data points result in lower uncertainty in final predictions.

The alluvial plain parameters have the strongest reduction in posterior spread. Therefore, it seems that our model estimates are dominated by these parameters. A downside of dominance of one or a set of parameters over the others is that it reduces the constraining power of the other parameters. On the other hand, it also realistically shows in our case that land subsidence in the alluvial plain, though not exhibiting the largest rates of subsidence in the area, is an important component in the Ravenna area. And, it is constrainable, with the large number of InSAR points available in the alluvial plain.

Even with a limited number of InSAR points, parameter optimization can yield valuable insights. For example, the  $C_s$  parameter of the paleo coast shows a significant reduction in subsidence rate from prior to posterior. Despite minimal improvement in parameter spread, the average parameter value indicates low subsidence rates for the paleo coast, aligning with prior expectations based on geological characteristics.

Certainly, an increased spread after ES-MDA should not always be viewed negatively (e.g. <sup>3</sup>). Narrow prediction bands do not guarantee better performance. A broader range of parameter values captures the complex interactions of subsidence more effectively, avoiding the constraints of a narrower, potentially unrealistic range. An increase may also be explained by the use of an inflation factor.

### 5.2.2. Correlations

Considering multiple processes causing land subsidence may introduce interdependence between parameters. Analyzing parameter correlations across the entire research area and the coastal strip enhances our understanding of these interdependencies and highlights local and regional differences. In the study on the entire research area, significant parameter correlations are absent, indicating the appropriateness of the chosen area size and model parameters.

In the coastal strip, a notable correlation exists between the industry factor and the  $C_s$  parameter of the lagoon. Industrial activity in the lagoon increases both the general building-related compaction and the industry factor. This stronger correlation in the coastal area, compared to the total research area, likely arises because the industry factor affects more data points across various geomorphological classes in the total research area. When the industry factor affects fewer geomorphological classes, the correlation with the remaining classes strengthens. Parameter correlations complicate the disentanglement of their relative contributions to subsidence. Thus, the parameters in Table 2 might not accurately show the relative contribution of different subsidence causes. While subarea results help us understand these interactions, the final

parameter values of the larger study area are considered more reliable.

# 5.2.3. Inflation factor

We employed an inflation factor of 1.9 to increase the parameter ensemble spread in our ES-MDA. This factor was determined empirically. Its value is higher than values reported in other publications on ensemble-based assimilation (e.g. <sup>48,85</sup>). However, the literature lacks coverage of the ensemble spread parameter inflation in ES-MDA applications.

The justification for this inflation factor is related to model limitations, the nature of observations, prior parameter uncertainty, and system non-linearity. These issues were also noted by Carrassi et al.  $^{21}$  and Bocquet and Sakov.  $^{13}$  Significant differences between model and data within the research area stem from processes not included in the model (e.g. groundwater extraction, tectonics), discrepancies between the model and reality (e.g. oversimplifications), and variations in the system (e.g. building-type).

Our research area exhibits great spatial variability, and includes a broad range of subsidence processes, which necessitates a larger inflation factor to accurately capture the complex dynamics. A large inflation factor ensures that the model remains flexible enough to accommodate variations and predictive capability. In areas like the region of Ravenna, where a combination of factors affects the total subsidence, a relatively large inflation factor might be beneficial to capture the nuanced subsidence processes effectively and prevent ensemble collapse. Interestingly, a smaller inflation factor suffices for the study on the subarea of the coastal strip, because the collapse is less severe. This could be due to the smaller number of observations, which as a result contain fewer spatial correlations because of lower spatial variability and less heterogeneity.

The simplicity of a basic inflation factor is a practical choice, simpler than alternative methods, such as a dynamic inflation error, <sup>56</sup> localization or Tikhonov regularization. <sup>26</sup> However, by addressing specific issues such as spurious correlations and solution stability, alternative methods could complement or surpass the performance with the inflation factor. Further studies are needed to explore the effectiveness and practicality of these alternative methods for subsidence studies.

# 5.3. Limitations and implications of the results

Previous studies on land subsidence in the Ravenna region have predominantly focused on the impacts of groundwater and gas extraction. <sup>10,35,33,63,66,71,72</sup> More recent contributions also assessed drainage and groundwater processes <sup>6,7,67</sup> and building related subsidence <sup>37</sup> as separate processes. Our results align with the findings of the previous studies focusing on separate contributors to subsidence. We indicate a minimal current influence of onshore groundwater extraction on subsidence (e.g. <sup>6,7</sup>). Additionally, gas extraction-induced subsidence from offshore fields has decreased over time and a minimal influence is indicated by on shore gas extraction in the north of the study area (e. g. <sup>66</sup>). We have extended our understanding of subsidence in the region by integrating the effects of building loads and industrial infrastructure into the modelling framework combined with the other modelled processes.

These findings have implications for the future development of the region, as structural weight has an important role in accelerating sediment compaction, particularly in reclaimed and lagoonal areas. By accounting for multiple contributing factors, the methodology presented here offers a framework that can support more targeted urban planning and infrastructure design. It may also inform regulatory strategies aimed at reducing subsidence risks by managing groundwater extraction and industrial activities, where relative sea-level rise is an important consequence of subsidence in the region (e.g. <sup>22</sup>).

Although we have successfully disentangled multiple subsidence processes in the Ravenna area, several limitations must be acknowledged. The current model simplifies the heterogeneity of building structures, does not explicitly account for groundwater extraction or drainage effects, and omits potentially relevant deep geodynamic influences. Soboyejo et al. 67 highlighted the role of drainage in increasing vertical seepage and subsidence in coastal drainage basins. Furthermore, Bertoni et al. 10 emphasized that land reclamation and associated drainage activities have contributed to ongoing subsidence in reclaimed areas. Future studies would benefit from incorporating high-resolution data on building characteristics, like a more extended approach of Grassi et al., <sup>37</sup> but including subsurface properties. Future studies should also integrate hydrogeological models and include structural geological constraints. The latter is generally ignored in subsidence studies of coastal and deltaic plains (e.g. 80). A combination of InSAR with GNSS and leveling data could further improve the spatial and temporal resolution of subsidence estimates, as recently done in the broader Emilia-Romagna region by Bitelli et al.. 11 Extending the time period of the dataset may also help to capture evolving trends in shallow and deep subsidence processes.

The implications of this study extend beyond the local context and are relevant to international challenges in urban planning, infrastructure development, environmental management, and policy-making. It emphasizes the necessity of understanding the interplay between diverse drivers of subsidence. Globally, subsidence is often the result of interacting factors such as building-related compaction, soil shrinkage and oxidation, and fluid extraction from the subsurface. Major cities including Bangkok, Jakarta, Mexico City, and Shanghai illustrate how these processes can interfere, exacerbated by rapid urbanization and geomorphological settings, to produce severe ground deformation. <sup>1,16</sup>, 55,86

Finally, the application of data assimilation techniques such as Ensemble Smoother with Multiple Data Assimilation (ES-MDA), particularly with higher inflation factors, is especially valuable in settings with complex subsidence dynamics. This approach would for example be relevant in regions like the Mekong Delta in Vietnam, <sup>47</sup> where overlapping shallow and deep drivers are present, as well as in the Groningen region in the Netherlands, where gas extraction-induced subsidence adds further complexity. <sup>76</sup>

# 6. Conclusions

This study has integrated a diverse range of datasets and land subsidence observations to evaluate the relative influence of various subsidence processes in the Ravenna area over the decade between 2012 and 2022. The analysis identified three primary components of subsidence, the combination of which can result in subsidence rates of over 10 mm/year:

- 1. Building cause: The built environment imposes subsidence on the research area. Industrial buildings contribute significantly more to subsidence than residential buildings. On average, industrial buildings cause subsidence rates that are two times higher than those of residential structures. This effect is even stronger in reclaimed areas, due to the nature of industrial activities there, combined with the geomorphological characteristics of the area. Here, subsidence rates increase by a factor eight with respect to residential buildings.
- Shallow cause: The impact of this process is found along the complete coastal strip. Driven by the weight of overburden on shallow tidal deposits and the drainage of reclaimed land, this process shows the fastest rates in reclaimed zones, aligning with findings from other coastal regions.
- 3. Deep cause: The subsidence bowl due to gas extraction activities offshore contributes to onshore subsidence locally in our study area.
- 4. Secondary to these main processes, drainage and groundwater extraction also appear to influence subsidence, particularly in inland areas. The historical extraction of groundwater for agricultural and industrial purposes, especially northwest of Ravenna, likely continues to contribute to subsidence, although it was not directly

- accounted for in our model. The contribution of these secondary processes is estimated to be less than 2–3 mm/year. Possibly, other deep causes not included in this analysis, such as tectonics, consolidation of Quaternary deposits, and glacial isostatic adjustment, would also marginally affect the area.
- 5. Our analysis demonstrates that understanding land subsidence in the Ravenna region requires a comprehensive approach that considers the interplay between geomorphology, industrialization, urbanization, and fluid extraction. A holistic view of subsidence processes can only be achieved by considering these factors collectively.
- 6. Key findings of our study can be summarized as follows:
- Combination of causes: The fastest subsidence rates are observed in areas where multiple subsidence processes coincide. In particular, the presence of heavy industry in locations with high soil compaction potential is driving high subsidence rates.
- Soil characteristics: The characteristics of the soil significantly influence both building-related and soil compaction. This highlights the need for detailed geotechnical assessments in subsidence-prone areas
- Model Improvements: To further improve our understanding of subsidence, model improvements are important. However, they largely rely on data availability. Therefore, measurement campaigns are imperative for improved subsidence mitigation.

In conclusion, this study underscores the importance of a multi-faceted approach to subsidence modeling, integrating various subsidence drivers and detailed local data. By enhancing our understanding of these complex interactions, more effective mitigation strategies can be developed to address subsidence issues in the Ravenna area and similar regions worldwide.

# CRediT authorship contribution statement

Manon Verberne: Writing – review & editing, Writing – original draft, Visualization, Validation, Software, Resources, Methodology, Investigation, Formal analysis, Data curation, Conceptualization. Pietro Teatini: Writing – review & editing, Supervision, Resources, Project administration, Funding acquisition, Conceptualization. Kay Koster: Writing – review & editing, Supervision, Funding acquisition. Peter Fokker: Writing – review & editing, Supervision, Project administration, Funding acquisition. Claudia Zoccarato: Writing – review & editing, Supervision.

# **Declaration of Competing Interest**

The authors declare the following financial interests/personal relationships which may be considered as potential competing interests: Manon Verberne reports financial support was provided by Dutch Research Council. Pietro Teatini reports financial support was provided by European Union. All authors declare that they have no known competing financial interests or personal relationships that could have appeared to influence the work reported in this paper.

### Acknowledgments

We are grateful to ENI for providing the necessary input data for this study, which includes the InSAR dataset and geomechanical modelling results. We are also grateful to the geological survey of the Emilia-Romagna Region (Luisa Perini and Paolo Severi) for assistance with acquiring necessary input data, which consists of the soil texture map and the dataset of CPTs. Furthermore, we would like to thank two anonymous reviewers for their useful comments. The research presented in this paper is part of the project Living on soft soils: subsidence and society (grant nr.: NWA.1160.18.259). This project is funded through the Dutch Research Council (NWO-NWA-ORC), Utrecht University,

Wageningen University, Delft University of Technology, Ministry of Infrastructure & Water Management, Ministry of the Interior & Kingdom Relations, Deltares, Wageningen Environmental Research, TNO-Geological Survey of The Netherlands, STOWA, Water Authority: Hoogheemraadschap de Stichtse Rijnlanden, Water Authority: Drents Overijsselse Delta, Province of Utrecht, Province of Zuid-Holland, Municipality of Gouda, Platform Soft Soil, Sweco, Tauw BV, NAM. This study was also carried out within the RETURN Extended Partnership and received funding from the European Union Next- GenerationEU (National Recovery and Resilience Plan-NRRP, Mission 4, Component 2, Investment 1.3—D.D. 1243 2/8/2022, PE.0000005).

### Open research

Data from the geological survey of the Emilia-Romagna Region<sup>57</sup> has been used for the lithostratigraphic analysis. The Global Human Settlement Layer from the European Commission<sup>25</sup> has been used to determine the 5-yearly differential building volumes. ENI has provided the processed InSAR dataset and the geomechanical model results. Figures were made with Matplotlib v.3.4.3 available under the matplotlib license at https://matplotlib.org and OGIS v3.24.

# Appendix A. Supporting information

Supplementary data associated with this article can be found in the online version at doi:10.1016/j.gete.2025.100710.

### Data availability

All data, code and models are freely available upon reasonable request, with some exceptions. We obtained InSAR and geomechanical modeling data related to gas extraction from a commercial operator (ENI, an Italian hydrocarbon company). While our modeled subsidence results based on this geomechanical data are provided in figure form in our manuscript, the raw data cannot be shared.

### References

- Abidin HZ, Andreas H, Gumilar I, Brinkman JJ. Study on the risk and impacts of land subsidence in Jakarta. Proc Int Assoc Hydrol Sci. 2015;372:115–120.
- Ahmed S, Hiraga Y, Kazama S. Land subsidence in Bangkok vicinity: Causes and long-term trend analysis using InSAR and machine learning. Sci Total Environ. 2024; 946, 174285.
- Akitaya K, Aichi M. Land Subsidence Model Inversion with the Estimation of Both Model Parameter Uncertainty and Predictive Uncertainty Using an Evolutionary-Based Data Assimilation (EDA) and Ensemble Model Output Statistics (EMOS). Water. 2024;16(3):423.
- Amorosi A, Colalongo M, Pasini G, Preti D. Sedimentary response to Late Quaternary sea-level changes in the Romagna coastal plain (northern Italy). *Sedimentology*. 1999;46(1):99–121. https://doi.org/10.1046/j.1365-3091.1999.00205.x.
- Anderson JL. Exploring the need for localization in ensemble data assimilation using a hierarchical ensemble filter. *Physica D Nonlinear Phenomena*. 2007;230(1-2): 99–111.
- Antoncecchi I, Ciccone F, Rossi G, et al. Soil deformation analysis through fluiddynamic modelling and DInSAR measurements. A focus on groundwater withdrawal in the Ravenna area (Italy). *Bull Geophys Oceanogr*. 2021;62(2):301–318. https:// doi.org/10.4430/bgta0350.
- Antonellini M, Giambastiani BMS, Greggio N, et al. Processes governing natural land subsidence in the shallow coastal aquifer of the Ravenna coast, Italy. CATENA. 2019; 172:76–86. https://doi.org/10.1016/j.catena.2018.08.019.
- Bau D, Gambolati G, Teatini P. Waterdrive dynamics and enhanced land subsidence over productive gas fields: Application to Dosso degli Angeli reservoir, Ravenna, Italy. Theory, Modeling, and Field Investigation in Hydrogeology. Geological Society of America; 2000. https://doi.org/10.1130/0-8137-2348-5.129.
- Bertoni W, Brighenti G, Gambolati G, Ricceri G, Vuillermin F. Land subsidence due to gas production in the on-and offshore natural gas fields of the Ravenna area. *Italy Int J Rock Mech Min Sci Geomech Abstr.* 1996;8(33):379A.
- Bertoni W, Elmi C, Marabini F. The subsidence of Ravenna. G di Geol Appl. 2005:1. https://doi.org/10.1474/GGA.2005-01.0-03.0003.
- Bitelli G, Ferretti A, Giannico C, et al. Subsidence monitoring in Emilia-Romagna Region (Italy) from 2016 to 2021: From InSAR and GNSS integration to data analysis. Remote Sens. 2025;17:947. https://doi.org/10.3390/rs17060947.

- Bjerrum L. Engineering geology of norwegian normally-consolidated marine clays as related to settlements of buildings. *Géotechnique*. 1967;17(2):83–118. https://doi. org/10.1680/geot.1967.17.2.83.
- Bocquet M, Sakov P. Combining inflation-free and iterative ensemble Kalman filters for strongly nonlinear systems. *Nonlinear Process Geophys.* 2012;19(3):383–399.
- Bondesan M, Favero V, Viñals MJ. New evidence on the evolution of the Po-delta coastal plain during the Holocene. Quat Int. 1995;29-30:105–110. https://doi.org/ 10.1016/1040-6182(95)00012-8.
- Bruno L, Campo B, Costagli B, et al. Factors controlling natural subsidence in the Po Plain. Living Subsid Proc X Int Symp Land Subsid P Fokker G Erkens eds Proc IAHS. 2020;382:285–290. https://doi.org/10.5194/piahs-382-285-2020.
- Cabral-Cano E, Dixon TH, Miralles-Wilhelm F, Díaz-Molina O, Sánchez-Zamora O, Carande RE. Space geodetic imaging of rapid ground subsidence in Mexico City. Geol Soc Am Bull. 2008;120(11-12):1556–1566.
- Candela T, Koster K. The many faces of anthropogenic subsidence. Science. 2022;376 (6600):1381–1382.
- Capasso G, Mantica S. Numerical Simulation of Compaction and Subsidence using ABAQUS. USA: Proceedings of the ABAQUS Users' Conference. Boston; 2006.
- Carbognin L, Gatto P, Mozzi G. In: Poland JF, ed. Case history no. 9.15: Ravenna, Italy. Guidebook to Studies of Land Subsidence due to Ground-Water Withdrawal; 1984:291–305.
- Carminati E, di Donato G. Separating natural and anthropogenic vertical movements in fast subsiding areas: The Po Plain (N.Italy) case. *Geophys Res Lett.* 1999;26: 2291–2294. https://doi.org/10.1029/1999GL900518, 1999.
- Carrassi A, Bocquet M, Bertino L, Evensen G. Data assimilation in the geosciences: An overview of methods, issues, and perspectives. Wiley Interdiscip. Rev.: Clim. Change. 2018;9(5), e535.
- Cerenzia I, Putero D, Bonsignore F, Galassi G, Olivieri M, Spada G. Historical and recent sea level rise and land subsidence in Marina di Ravenna, northern Italy. *Ann Geophys.* 2016;59(5):P0546. https://doi.org/10.4401/ag-7022.
- Chaussard E, Wdowinski S, Cabral-Cano E, Amelung F. Land subsidence in central Mexico detected by ALOS InSAR time-series. Remote Sens Environ. 2014;140:94–106.
- Den Haan EJD. A compression model for non-brittle soft clays and peat. *Géotechnique*. 1996;46(1):1–16. https://doi.org/10.1680/geot.1996.46.1.1.
- European Commission. Joint Research Centre. (2023). GHSL data package 2023.
   Publications Office of the European Union. (https://data.europa.eu/doi/10.2760/098587).
- Evensen G. Data Assimilation: The Ensemble Kalman Filter. Springer Science & Business Media; 2009. https://doi.org/10.1007/978-3-642-03711-5.
- Fiaschi S, Tessitore S, Boni R, Di Martire D, Achilli V, Borgstrom S, Calcaterra D. From ERS-1/2 to Sentinel-1: two decades of subsidence monitored through A-DInSAR techniques in the Ravenna area (Italy). GIScience Remote Sens. 2016;54(3): 305–328. https://doi.org/10.1080/15481603.2016.1269404.
- Floris M, Fontana A, Tessari G, Mulè M. Subsidence zonation through satellite interferometry in coastal plain environments of NE Italy: a possible tool for geological and geomorphological mapping in urban areas. *Remote Sens.* 2019;11(2): 165.
- Fokker PA, Gunnink JL, Koster K, de Lange G. Disentangling and parametizing shallow sources of subsidence: application to a reclaimed coastal area, Flevoland, the Netherlands. *J Geophys Res Earth Surf.* 2019;124:1099–1117.
- Fokker PA, Wassing BBT, Van Leijen FJ, Hanssen RF, Nieuwland DA. Application of an ensemble smoother with multiple data assimilation to the Bergermeer gas field, using PS-InSAR. Geomech Energy Environ. 2016;5:16–28.
- Galloway DL, Burbey TJ. Regional land subsidence accompanying groundwater extraction. *Hydrogeol J.* 2011;19(8):1459–1486. https://doi.org/10.1007/s10040-011-0775-5.
- 32. Galloway, D.L., Jones, D.R., & Ingebritsen, S.E. (Eds.). (1999). Land subsidence in the United States (Vol. 1182). Geological Survey (USGS)..
- Gambolati G, Ricceri G, Bertoni W, Brighenti G, Vuillermin E. Mathematical simulation of the subsidence of Ravenna. Water Resour Res. 1991;27(11): 2899–2918
- Gambolati G, Teatini P, Tomasi L, Gonella M. Coastline regression of the Romagna Region, Italy, due to natural and anthropogenic land subsidence and sea level rise. Water Resour Res. 1999;35(1):163–184. https://doi.org/10.1029/1998WR900031.
- 35. Gambolati G, Teatini P. Numerical analysis of land subsidence due to natural compaction of the Upper Adriatic Sea basin. In CENAS: Coastline Evolution of the Upper Adriatic Sea Due to Sea Level Rise and Natural and Anthropogenic Land Subsidence. Springer; 1998:103–131.
- Gazzola L, Ferronato M, Teatini P, et al. Reducing uncertainty on land subsidence modeling prediction by a sequential data-integration approach. Appl Arlua shore Reserv Italy Geomech Energy Environ. 2023;33, 100434.
- Grassi F, Mancini F, Bassoli E, Vincenzi L. Contribution of anthropogenic consolidation processes to subsidence phenomena from multi-temporal DInSAR: a GIS-based approach. GIScience Remote Sens. 2022;59(1):1901–1917. https://doi. org/10.1080/15481603.2022.2143683.
- Hendricks Franssen HJ, Kinzelbach W. Real-time groundwater flow modelling with the ensemble Kalman filter: joint estimation of states and parameters and the filter inbreeding problem. Water Resour. Res. 2008;44(9), W09408.
- Janna C, Castelletto N, Ferronato M, Gambolati G, Teatini P. A geomechanical transversely isotropic model of the Po River basin using PSInSAR derived horizontal displacement. Int J Rock Mech Min Sci. 2012;51:105–118.
- Ketelaar VBH. Subsidence due to hydrocarbon production in the Netherlands. In Satellite Radar Interferometry. Subsidence Monitoring Techniques. Springer; 2009:7–26.
- Koster K, Stafleu J, Stouthamer E. Differential subsidence in the urbanised coastaldeltaic plain of the Netherlands. Neth J Geosci. 2018;97(4):215–227.

- Li F, Liu G, Tao Q, Zhai M. Land subsidence prediction model based on its influencing factors and machine learning methods. *Nat Hazards*. 2023;116(3): 2015.
- Lunne, T., Powell, J.J.M., & Robertson, P.K. (2002). Cone penetration testing in geotechnical practice. CRC Press.
- Maselli V, Trincardi F. Large-scale single incised valley from a small catchment basin on the western Adriatic margin (central Mediterranean Sea). Glob. Planet. Change. 2013;100:245–262.
- Maselli V, Trincardi F. Man made deltas. Sci Rep. 2013;3(1):1926. https://doi.org/ 10.1038/srep01926.
- Meckel TA, Ten Brink US, Williams SJ. Sediment compaction rates and subsidence in deltaic plains: numerical constraints and stratigraphic influences. Basin Res. 2007;19 (1):19–31. https://doi.org/10.1111/j.1365-2117.2006.00310.x.
- Minderhoud PS, Erkens G, Pham VH, et al. Impacts of 25 years of groundwater extraction on subsidence in the Mekong delta, Vietnam. *Environ Res Lett.* 2017;12(6), 064006. https://doi.org/10.1088/1748-9326/aa7146.
- Miyoshi T, Sato Y, Kadowaki T. Ensemble Kalman filter and 4D-Var intercomparison with the Japanese operational global analysis and prediction system. *Mon Weather Rev.* 2010;138(7):2846–2866. https://doi.org/10.1175/2010MWR3209.1.
- Moreno-Maroto JM, Alonso-Azcárate J. Evaluation of the USDA soil texture triangle through Atterberg limits and an alternative classification system. *Appl Clay Sci.* 2022;229, 106689. https://doi.org/10.1016/j.clay.2022.106689.
- Morton RA, Bernier JC, Barras JA. Evidence of regional subsidence and associated interior wetland loss induced by hydrocarbon production, Gulf Coast region, USA. Environ Geol. 2006;50(2):261–274. https://doi.org/10.1007/s00254-006-0207-3.
- Neumann B, Vafeidis AT, Zimmermann J, Nicholls RJ. Future coastal population growth and exposure to sea-level rise and coastal flooding – A global assessment. PLOS ONE. 2015;10(3), e0118571. https://doi.org/10.1371/journal.pone.0118571.
- Nicholls RJ, Lincke D, Hinkel J, et al. A global analysis of subsidence, relative sealevel change and coastal flood exposure. Nat Clim Change. 2021;11(4):338–342.
- Pesaresi, M. (2023b). GHS-BUILT-H R2023A GHS building height, derived from AW3D30, SRTM30, and Sentinel2 composite (2018). European Commission, Joint Research Centre (JRC). (https://data.europa.eu/89h/85005901-3a49-48dd-9d19-62 613E465fs)
- Pesaresi M, Politis P. GHS-BUILT-V R2023A GHS built-up volume grids derived from joint assessment of Sentinel2, Landsat, and global DEM data, multitemporal. European Commission, Joint Research Centre (JRC); 2023:1975–2030. (https://data.europa. eu/89h/ab2f107a-03cd-47a3-85e5-139d8ec63283).
- Phien-wej N, Giao PH, Nutalaya P. Land subsidence in Bangkok, Thailand. Eng Geol. 2006;82(4):187–201. https://doi.org/10.1016/j.enggeo.2005.10.004.
- Raanes PN, Bocquet M, Carrassi A. Adaptive covariance inflation in the ensemble Kalman filter by Gaussian scale mixtures. Q J R Meteorol Soc. 2019;145(718):53–75. https://doi.org/10.1002/gi.3386.
- 57. Regione Emilia Romagna. (2024). Water resources. Retrieved September 12, 2024, from (https://ambiente.regione.emilia-romagna.it/en/geologia/geology/water-reso
- Robertson PK. Soil classification using the cone penetration test. Can Geotech J. 1990;27(1):151–158. https://doi.org/10.1139/t90-014.
- Robertson PK. Interpretation of cone penetration tests a unified approach. Can Geotech J. 2009;46(11):1337–1355. https://doi.org/10.1139/T09-065.
- Ronchi L, Fontana A, Cohen KM, Stouthamer E. Late Quaternary landscape evolution of the buried incised valley of Concordia Sagittaria (Tagliamento River, NE Italy): A reconstruction of incision and transgression. *Geomorphology*. 2021;373, 107509. https://doi.org/10.1016/j.geomorph.2020.107509.
- 61. Roncuzzi A. Ravenna nei tempi antichi. Cl e Ravenna. 1986;3(1-2):2-4.
- Schmidt CW. Delta subsidence: An imminent threat to coastal populations. Environ Health Perspect. 2015;123(8):A204–A209. https://doi.org/10.1289/ehp.123-A204.
- Health Perspect. 2015;123(8):A204–A209. https://doi.org/10.1289/ehp.123-A204.
  63. Schroot, B.M., Fokker, P.A., Lutgert, J.E., Van der Meer, B. G. H., Orlic, B., Scheffers, B. C., & Barends F.B.J. (2005) Subsidence induced by gas production: an integrated approach. In: Proc SISOLS'05, special volume, geodelft, Millpress Rotterdam, pp 121–135.
- Segall P, Grasso JR, Mossop A. Poroelastic stressing and induced seismicity near the Lacq gas field, southwestern France. *J Geophys Res Solid Earth*. 1994;99(B8): 15423–15438. https://doi.org/10.1029/94JB00989.
- Shirzaei M, Freymueller J, Törnqvist TE, Galloway DL, Dura T, Minderhoud P. Measuring, modelling and projecting coastal land subsidence. Nat Rev Earth Environ. 2021;2(1):40–58.
- Simeoni U, Tessari U, Corbau C, Tosatto O, Polo P, Teatini P. Impact of land subsidence due to residual gas production on surficial infrastructures: The Dosso degli Angeli field study (Ravenna, Northern Italy). Eng Geol. 2017;229:1–12. https://doi.org/10.1016/j.enggeo.2017.09.008.
- Soboyejo LA, Giambastiani BMS, Molducci M, et al. Different processes affecting long-term Ravenna coastal drainage basins (Italy): implications for water

- management. Environ Earth Sci. 2021;80:493. https://doi.org/10.1007/s12665-021-00774.5
- Strozzi T, Carreon-Freyre D, Wegmüller U. Land subsidence and associated ground fracturing: study cases in central Mexico with ALOS-2 PALSAR-2 ScanSAR Interferometry. Proc Int Assoc Hydrol Sci. 2020;382:179–182.
- Syvitski JP. Deltas at risk. Sustain Sci. 2008;3:23–32. https://doi.org/10.1007/ s11625-008-0043-3
- Tarocco, P., Staffilani, F., & Ungaro, F. (2015). CARTA DELLA TESSITURA DEI SUOLI DELLA PIANURA EMILIANO-ROMAGNOLA STRATO 0-30 cm. Region Emilia-Romagna, Servizio Geologico, Sismico e dei Suoli. (https://mappegis.regione.emilia -romagna.it/gstatico/documenti/dati\_pedol/tessitura\_pianura.pdf).
- Teatini P, Ferronato M, Gambolati G, Bertoni W, Gonella M. A century of land subsidence in Ravenna, Italy. Environ Geol. 2005;47(6):831–846. https://doi.org/ 10.1007/s00254-004-1215-9.
- Teatini P, Ferronato M, Gambolati G, Gonella M. Groundwater pumping and land subsidence in the Emilia-Romagna coastland, Italy: Modeling the past occurrence and the future trend. Water Resour Res. 2006;42:W01406. https://doi.org/10.1029/ 2005WR004242.
- Teatini P, Gambolati G, Tomasi L. Simulation of land subsidence due to gas production at Ravenna coastline. In Water Science and Technology Library. Springer Netherlands; 1998:133–150. https://doi.org/10.1007/978-94-011-5147-4\_6.
- Tosi L, Teatini P, Carbognin L, Brancolini G. Using high resolution data to reveal depth-dependent mechanisms that drive land subsidence: The Venice coast, Italy. Tectonophysics. 2009;474(1-2):271–284. https://doi.org/10.1016/j. tests. 2009.03.036
- van Thienen-Visser K, Fokker PA. The future of subsidence modelling: Compaction and subsidence due to gas depletion of the Groningen gas field in the Netherlands. Neth J Geosci. 2017;96(5):s105–s116. https://doi.org/10.1017/njg.2017.10.
- van Thienen-Visser K, Pruiksma JP, Breunese JN. Compaction and subsidence of the Groningen gas field in the Netherlands. *Proc Int Assoc Hydrol Sci.* 2015;372:367–373. https://doi.org/10.5194/piahs-372-367-2015.
- Veggiani A. Le variazioni della linea di costa del Ravennate dall'Età Preromana al Medioevo. Cent di Cult Sull'arte Ravenn e Biz Ravenna. 1976;23:331–344.
- Verberne M. Disentangling Subsidence Towards a holistic approach. PhD Thesis. Utrecht University, Faculty of Geosciences. USES; 2025;348. ISBN: 978-90-6266-722-2.
- Verberne M, Koster K, Fokker PA. Multi-data settlement prediction along a road section integrating InSAR and coastal subsurface information with data assimilation. Front Earth Sci. 2024;11, 1323874. https://doi.org/10.3389/feart.2023.1323874.
- Verberne M, Koster K, De Bresser H, Fokker PA. Fifty Years of Intermediate-Depth Compaction in the Coastal Plain of the Netherlands: Detailed Analysis of Twenty Extensometers. J Surv Eng. 2025;151(3):05025002.
- Verberne M, Koster K, Lourens A, Gunnink J, Candela T, Fokker PA. Disentangling shallow subsidence sources by data assimilation in a reclaimed urbanized coastal plain, South Flevoland polder, the Netherlands. *J Geophys Res Earth Surf.* 2023;128 (7), e2022JF007031. https://doi.org/10.1029/2022JF007031.
- Visschendijk, M.A.T., & Trompille, V. (2009). MSettle Version 8.2. Embankment design and soil settlement prediction. *Deltares report*. (https://repository.tudelft.nl/islandora/object/uuid:88aa11df-55a9-4266-89f1-aefb5568dca2?collection=resear ch).
- Vitagliano E, Riccardi U, Piegari E, Boy JP, Di Maio R. Multi-component and multisource approach for studying land subsidence in deltas. *Remote Sens.* 2020;12(9): 1465.
- 84. Vos P. Origin of the Dutch coastal landscape: Long-term landscape evolution of the Netherlands during the Holocene, described and visualized in national, regional and local palaeogeographical map series. Barkhuis; 2015.
- Whitaker JS, Hamill TM. Ensemble data assimilation without perturbed observations. Mon Weather Rev. 2002;130(7):1913–1924. https://doi.org/10.1175/ 1520-0493(2002)130<1913:EDAWPO>2.0.CO;2.
- **86.** Ye S, Xue Y, Wu J, Yan X, Yu J. Progression and mitigation of land subsidence in China. *Hydrogeol J.* 2016;24(3):685–706.
- Zhang Y, Huang H, Liu Y, Liu Y. Self-weight consolidation and compaction of sediment in the Yellow River Delta, China. Phys Geogr. 2018;39(1):84–98.
- Zhang Y, Wu H, Li M, Kang Y, Lu Z. Investigating ground subsidence and the causes over the whole Jiangsu Province, China using sentinel-1 SAR data. *Remote Sens*. 2021;13(2):179.
- Zoccarato C, Bau D, Ferronato M, Gambolati G, Alzraiee A, Teatini P. Data assimilation of surface displacements to improve geomechanical parameters of gas storage reservoirs. J Geophys Res Solid Earth. 2016;121(3):1441–1461.
- Zoccarato C, Minderhoud PS, Teatini P. The role of sedimentation and natural compaction in a prograding delta: Insights from the mega Mekong delta. Vietnam Sci Rep. 2018;8(1):11437.